LBL-11102
CONF-8007192--1

Lawrence Berkeley Laboratory
UNIVERSITY OF CALIFORNIA

Invited talk presented at the 1980 Institute for Nuclear Studies, Kikuchi Summer School on Nuclear Physics at High Energies, Fuji-Yoshida, Japan, July 1-4, 1980

HIGH ENERGY NUCLEAR COLLISIONS IN THE FEW GeV/NUCLEON REGION--PROJECTILE AND TARGET FRAGMENTATION

L. S. Schroeder

June 1980

MASTER

DISTRIBUTION OF THIS DOCUMENT IS UNLIMITED

Supported by the U.S. Department of Energy under Contract W-7405-ENG-48

HIGH ENERGY NUCLEAR COLLISIONS IN THE FEW GeV/NUCLEON REGION--PROJECTILE AND TARGET FRAGMENTATION*

L. S. Schroeder

Lawrence Berkeley Laboratory, Berkeley, California 94720
University of California

ABSTRACT

A general review of nucleon-nucleus and nucleus-nucleus collisions for incident energies <10 GeV/nucleon will be presented. I will briefly discuss the division of these interactions into peripheral and central collisions. The talk will cover such subjects as: target and projectile fragmentation systematics, production of exotic nuclear fragments, studies of multi-particle final states, total cross section measurements, results from an experiment which indicate the production of projectile fragments with an anomalously short reaction mean-free-path, high energy particle production at backward angles beyond simple N-N kinematic limits, and recent results on backward particle emission in studies with the Berkeley streamer chamber. In each topic, I will try and emphasis both the particle and nuclear physics aspects which are present. A brief discussion of future trends in this energy range will end the presentation.

DISCLAIMER

This report was prepared as an account of work sponsored by an agency of the United States Government. Neither the United States Government nor any agency thereof, nor any of their employees, makes any warranty, express or implied, or assumes any legal liability or responsibility for the accuracy, completeness, or usefulness of any information, apparatus, product, or process disclosed, or represents that its use would not infringe privately owned rights. Reference herein to any specific commercial product, process, or service by trade name, trademark, manufacturer, or otherwise, does not necessarily constitute or imply its endorsement, recommendation, or favoring by the United States Government or any agency thereof. The views and opinions of authors expressed herein do not necessarily state or reflect those of the United States Government or any agency thereof.

*This work is supported by the Nuclear Physics Division of the U. S. Department of Energy under Contract No. W-7405-ENG-48.

DISTRIBUTION OF

INTRODUCTION

The material for my talk will consist of a general review of nucleon-nucleus (N-A) and nucleus-nucleus (A-A) collisions for incident energies of <10 GeV/nucleon. The bulk of data in this energy range have come from the Dubna Synchrophasotron which can provide beams of $A \geq 2$ with energies up to about 4 GeV/nucleon, the Berkeley Bevalac Facility with energies up to 2.1 GeV/nucleon and Saturne at Saclay with energies up to 1.5 GeV/nucleon.

In the study of N-A and particularly A-A collisions it has become customary to divide the physics to be studied into two broad categories corresponding to peripheral and central collisions. Figure 1[1-3] provides a useful picture for displaying the concepts of interest. The invariant cross-section, $Ed^3\sigma/dp^3$, for the production of protons at 0° and 180° is plotted against the laboratory momentum of the outgoing proton. Several distinctive features are evident:

1) A peak centered about the momentum/nucleon of the projectile, which can primarily be associated with properties of the projectile, i.e., the region of projectile fragmentation.
2) An increase of the production cross section as the laboratory momentum approaches zero (rapidity = 0), indicative of a region which can be associated with the target, i.e., the region of target fragmentation.
3) In between these two regions (which primarily reflect the characteristic of the projectile/target nuclei) we find a region of relatively slow variation in cross section. This can be thought of as the mid-rapidity or central collision region ($y = 1/2 \ln (E + p_{\parallel}/E - p_{\parallel})$).

These separate fragmentation regions are studied most effectively via peripheral interactions; that is, with large impact parameters. One anticipates that these regions will be dominated by few-nucleon physics. Although at the extreme momenta of Fig. 1, a transition to a region where more nucleons of the target and/or projectile participate is clearly possible (at the kinematic boundaries total participation of all nucleons is of course required). Continuing with this approach, we would expect the central region to correspond to small impact parameters, involving the participation of a majority of the overlapping nucleons in the target and projectile. To further

high-light the idea of separating the interaction zones by large and small impact parameters, let us look at an example of each as seen in streamer chamber photos. Figure 2(a) shows the interaction of an 0.8 GeV/nucleon ^{12}C projectile with a target located inside the LBL streamer chamber. Six charged fragments are observed to exit the interaction, all moving fast (approximately at beam momentum/nucleon) in a small forward cone. No fragments from the target are seen, suggesting that this interaction was highly peripheral, involving relatively small energy/momentum transfers. In Fig. 2(b) the interaction of a high energy ^{40}Ar projectile with the target nucleus leads to a very large multiplicity final state. The distribution of final state particles in energy and angle suggests that there was substantial involvement of both projectile and target nucleons, i.e., a central collision event.

The subject matter for my talk will be largely drawn from existing data and interpretations of peripheral N-A and A-A collisions. The area of central collisions will be described elsewhere in this conference.[4] A brief list of the topics to be presented is shown below:

1) Target and projectile fragmentation systematics, including production of exotic nuclei,
2) total cross section and mean-free path measurements,
3) high energy $\pi^{\pm}$, p production in the backward direction, particularly production beyond simple N-N kinematic limits.

In each of these topics I will try to address both the particle and nuclear physics aspects of these studies. I will not be reviewing the many experiments in N-A collisions above 10 GeV which have been used to explore such areas as diffraction dissociation (e.g., $nA \rightarrow \pi^- pA$, $pA \rightarrow p\pi^+\pi^- A$) or the space-time development of hadronic matter in a nuclear enviroment.[5] However, diffraction dissociation as manifested in A-A collisions will be presented.

PROJECTILE FRAGMENTATION

The plan in this section will be to investigate features of peripheral collisions primarily observed in A-A collisions. When bombarding energies are 1-2 GeV/nucleon, the rapidity interval between target and projectile is 1 or 2 units of rapidity. With this separation the two regions of fragmentation can be thought of as independent (which is essentially the concept of limiting fragmentation that will be discussed later). Thus one is free to study the fragmentation process of either target or projectile, the choice being one of experimental technique. That is, projectile fragments will tend to be fast, forward-going fragments. Whereas, target fragments are generally low energy in the laboratory (target) frame, except for high energy tails which are known to exist.

A. Projectile Fragmentation Systematics

First, I want to demonstrate some of the general features that have been uncovered in the fragmentation of light heavy-ions (C, N, O, . . .) at the Berkeley Bevalac. This work involves studying the single-particle inclusive spectrum of fragments emitted near 0°.

Figure 3 shows a typical momentum spectrum for the fragmentation of a 2.1 GeV/nucleon ^{16}O projectile into carbon isotopes.[6] The cross section (in arbitary units) is plotted against the rigidity (p/z) of the fragment. The prominent peaks are experimentally identified as various isotopes of carbon. If one transforms any one of these distributions into the rest frame of the projectile, a Gaussian distribution is obtained which is peaked near zero momentum in that frame. Figure 4 shows such a distribution, this time for the fragmentation of a 2.1 GeV/nucleon ^{12}C projectile into ^{10}Be. This feature of a Gaussian-shaped momentum distribution is found to be relatively independent of projectile and target.

From these single-particle inclusive studies the following regularities have emerged:

1) For a majority of detected fragments, the momentum distributions can be parameterized in the projectile rest frame as:

$$\frac{d^3}{dp^3} = ce^{-(p_T^2/2\sigma_T^2)} e^{-((p_\parallel - \langle p_\parallel \rangle)^2/2\sigma_\parallel^2)} ,$$

where p_T and $p_\parallel$ are the transverse and longitudinal momentum of the fragment, $\langle p_\parallel \rangle$ is the value of the offset from zero momentum, and σ_T and $\sigma_\parallel$ are the FWHM for the transverse and longitudinal momentum distributions. Within the estimated errors,[6] $\sigma_T = \sigma_\parallel$.

2) The distribution of $\sigma_\parallel$ as a function of fragment mass F is in good agreement with the parabolic form $\sigma_\parallel^2 = \sigma_0^2 F(A - F)/(A - 1)$, where A is the mass of the projectile. This behavior is expected essentially on the basis of momentum conservation and lack of correlations between nucleons inside the fragmenting projectile. An example of this parabolic dependence is shown in Fig. 5. The term σ_0^2 can be related to the square of the Fermi momentum of the fragment.[7] Typically, one gets values in the range of 70-90 MeV/c, consistent with known information on nuclear momentum distributions.

3) The fragmentation cross section is found to factor into a target and projectile related part. If we write the reaction as, $A + B \rightarrow C + X$, then this factorization can be expressed as:

$$\sigma_{AB}^C = \gamma_A^C \gamma_B ,$$

where γ_A^C depends only on the projectile and the detected fragment, and γ_B depends only on the target. A dependence of $\gamma_B \propto B^{1/4}$, suggestive of a peripheral interaction, has been found.[6] It is also possible to parameterize the cross section as $\gamma_B \propto (A^{1/3} + B^{1/3} - \varepsilon)$, where ε plays the role of an overlap parameter.

There have been a number of theoretical models which have been brought forth to explain the regularities observed for projectile fragmentation. Feshbach and Huang[8] have applied a statistical model in association with "virtual clusters" to

explain the data. Goldhaber[7] has shown that the parabolic shape of $\sigma_{\parallel}^2$ could be understood in the context of thermodynamic models. Within the frame work of these models, the temperature of the emitting source is found to be about 8 MeV. An extension of the earlier abrasion-ablation model[9] has been developed to understand the dynamics of the projectile fragmentation process. In this model,[10] the fragmentation occurs in two stages. In the first, the abrasion stage, the overlapping nuclear matter is sheared away from both target and projectile. The remaining pre-fragment has a recoil momentum proportional to the Fermi momentum. This remaining pre-fragment is left in an excited state and subsequently decays into nucleons and/or nucleon clusters, which is the ablation stage. It is one of these fragments which is detected. The approach was to use a Glauber model to treat the first or abrasion stage. The following expression was obtained from the Glauber model for the cross section for n nucleons to be scattered out of the projectile (A) in a high energy A-A collision:

$$\sigma_n = \binom{A}{n} \int d^2b (1 - P(b))^n \, P(b)^{A-n} \qquad (1)$$

where

$$P(b) = \int dz d^2s \rho_A(s - bz) \exp[-A_t \sigma_{NN} \int dz' \rho_t(x,z')] \quad .$$

Here $(1 - P(b))$ is the probability of finding a projectile nucleon in the overlap region of the target (A_t) and projectile with impact parameter b. The equation thus represents the cross section for n projectile nucleons to be inside the overlap region and (A-n) to be outside. It is these (A-n) nucleons which are the pre-fragment. For the ablation stage they assume thermalization of the pre-fragment and compound nucleus decay (standard evaporation calculation). This two-step model generally is able to reproduce the fragmentation cross sections and the isotopic dependence for the observed widths of the momentum distributions. Note that the model has an energy dependence which is built in via the energy dependence of σ_{NN} (the nucleon-nucleon cross section).

For projectiles in the range of 1-2 GeV/nucleon the momentum widths and production cross section for various fragments are known to be relatively constant. As the energy of the projectile is reduced one anticipates a break in this trend, which could reflect directly on the reaction mechanisms responsible for the fragmentation. These fragmentation processes have been studied at much lower energies.[12,13] Figure 6 shows energy spectra for ^{12}C fragments produced in the reactions of ^{16}O on Au and Pb targets at incident energies of 8.75, 13.63, 15.63 and 19.7 MeV/nucleon.[12] All the spectra have a Gaussian-like shape with a maximum close to the energy, E_p, of the fragment moving with the same velocity as the incident projectile. Upon parameterizing these[12] and other data[13] at slightly higher energy in the form of Gaussians in momentum, the resulting energy dependence of the momentum widths σ_0^2 is displayed in Fig. 7. A saturation is seen to set in above 20 MeV/nucleon. The momentum widths can be related to the temperature T of a decaying system using $1/2\ T = \sigma_0^2/2\ m$ (where m = nucleon mass and $\sigma_0^2 = (P_{frag}/5)^2$). The corresponding temperature is shown on the right-hand side of Fig. 7 and is about 8 MeV. It has been conjectured[14] that below 20 MeV/nucleon there is longer time for equilibration to take place (compared to a fast process for $E > 20$ MeV/nucleon), and one naturally expects smaller temperatures. The dashed curve of Fig. 7 was obtained using a Fermi gas model for a system at a temperature T = 2 MeV. Both this thermal picture and the one previously discussed (abrasion-ablation) are consistent with the existing data.

An additional feature of the data seen at intermediate energies (near 100 MeV/nucleon) is the appearance of a surprisingly large transverse-momentum width to projectile fragments,[13] all nearly larger than 200 MeV/c. This is in sharp contrast to the 1-2 GeV/nucleon results where $\sigma_{p_\parallel} = \sigma_{p_\perp}$ to within 10 percent. The origin of these increased widths can be understood if one includes the fact that the projectile can experience an orbital deflection due to its interaction with the combined Coulomb-nuclear field of the target before the on-set of fragmentation. This additional contribution to the total width $\sigma_{p_\perp}$ will become more important as the energy is lowered. Extending the derivations of Goldhaber[7] to include orbital deflection, one obtains:

$$\sigma_p^2 (F) = \frac{F(A - F)}{(A - 1)} \sigma_1^2 + \frac{F(F - 1)}{A(A - 1)} \sigma_2^2 \quad , \tag{2}$$

where $\sigma_1^2 = 1/2\langle p_{i\perp}^2 \rangle = \sigma_o^2$ is the usual term due to <u>intrinsic</u> nucleon motion, and $\sigma_2^2 = 1/2\langle p_{A\perp}^2 \rangle$ is the variance of transverse momentum of the projectile at the time of fragmentation. Typical values of $\sigma_1 \sim$ 80-90 MeV/c (consistent with what is expected from $\sigma_{p_\parallel}$ results at 1-2 GeV/nucleon) and $\sigma_2 \sim$ 180-220 MeV/c were obtained. Theoretical calculations[13] for the orbital dispersion term are in reasonably agreement with the values obtained from fitting the data with Eq. (2).

B) <u>Some Current and Future Single-Particle Projectile (A ≥ 12) Fragmentation Studies</u>

Much of the projectile fragmentation process can apparently be understood in terms of the geometry of the collision, N-N and N-A cross sections, ground state properties of nuclei and the decay of a system which is excited to a temperature typically <8-12 MeV. None of these ideas are fundamentally new by themselves, but we shall see that they do provide a tool, the fragmentation process, which is of considerable utility to a broad range of nuclear and astrophysics problems.

First, if we consider the process of projectile fragmentation, we see that there are a number of advantages provided by doing the experiment at high energy. The fragments are emitted at energies typically near the beam velocity and are collimated into a narrow forward cone (at 2.1 GeV/nucleon subtending an angle of about 2° in the laboratory frame). Recently an experiment to study the production of neutron-rich isotopes far from the valley of stability shown in Fig. 8 was undertaken. Typically, neutron-rich isotopes have been made at low energy machines, usually requiring large amounts of running time. By doing the experiment at high energies,[15] where thick targets could be used together with the persistance of fragment velocity, the discovery of many new neutron-rich light isotopes was made possible with a relatively modest amount of accelerator time. Figure 9 shows a sample histogram of data from the bombardment of a Be target by a 212 MeV/nucleon ^{48}Ca beam. Such studies are able to test various mass formulae and check for the existence or non-existence of new isotopes, thereby testing the limits of stability of nuclei.

The systematics of projectile fragmentation also lends itself to the possibility of creating secondary beams of isotopes which can then be delivered in a controlled fashion to an experimental area for study. One group[16] at the Bevalac proposes to study the β-decay of exotic, neutron-rich nuclei produced by fragmentation and has demonstrated the feasibility of this scheme in a trial run.

Figure 10 shows cross sections for one-nucleon removal processes in the fragmentation of ^{12}C and ^{16}O beams. The dependence on target mass (A_T) is found to follow the average behavior for lighter emitted fragments observed in such experiments up to Cu. For heavier targets, a strong deviation from this average behavior is observed and is found to be proportional to Z^2, suggesting that Coulomb dissociation plays a major role. A simple model using the Weizsacker-Williams approximation was able to explain the single-nucleon removal data. In this model, the cross section for single-nucleon removal is given by:

$$\sigma_{WW} = \int \sigma(\omega)\ N(\omega)\ d\omega \quad , \tag{3}$$

where σ_{WW} is the cross section of interest, $\sigma(\omega)$ is the photonuclear cross section as a function of photon frequency ω, and $N(\omega)$ is the density of photons obtained by using the Weizsacker-Williams techniques. By measuring σ_{WW} one can invert the integral above and obtain $\sigma(\omega)$. For example, a group[17] at the Bevalac has proposed a measurement of the reaction, $^{18}O \rightarrow p + {}^{17}N$, on heavy targets in order to extract the virtual photon-weighted cross sections as a function of the photon-excitation energy. In effect, they hope that for single-nucleon removal fragmentation events the interaction essentially sees only the virtual photon field of the target nucleus. This in effect provides them with a "photon target" as shown below:

$$^{18}O + \text{"}\gamma\text{"} \rightarrow {}^{17}N + p \quad .$$

heavy target

The measurements of fragmentation cross sections over as complete a range of energies as possible is of particular

importance to cosmic-ray and astro-physical studies. Questions concerning the elemental abundances in the cosmic-ray spectrum and inter-stellar propagation mechanisms need such data as input.

Finally, beams of heavy-ions are proving of considerable use in both bio-medical studies and as a possible therapy tool. The possibility exists of fragmenting a primary heavy-ion beam and selecting out from its many fragmentation products a radioactive beam (e.g., $^{12}C \rightarrow {}^{11}C$). Such a beam could then be delivered and implanted in a patient in a well localized site to help in appropriate medical studies.

C. Single-Particle Fragmentation Studies of High Energy Deuterons and Alphas

Now we will consider the fragmentation of light nuclear systems; namely, deuterons and alphas. Being few-nucleon systems, one hopes to directly apply some of the concepts which have been found to be useful in high energy hardon collisions. Even at energies of a few GeV/nucleon, the energies are large compared to the characteristic energies (binding energies) of the system, and such concepts as limiting fragmentation might be applicable. From a nuclear physics view-point, the fragmentation process can potentially provide valuable information both on the internal structure and momentum distribution of constituents inside fragmenting nuclei.

Anderson et al.[1-2] have studied the forward fragmentation of deuterons and alphas over a wide range of incident energies and target material. We will concentrate our attention on the results from the reaction, $\alpha + A \rightarrow p + x$. Figure 11 shows the invariant cross section for proton production in a 2.1 GeV/nucleon alpha interaction with carbon. The data are shown for values of p_T of the outgoing proton between 0.0 and 0.58 GeV/c. The fragmentation peak (leading particle effect) persists until about 0.44 GeV/c, where only a shoulder appears. In each case, a high momentum tail (approximately exponential) is observed, perhaps indicating a different production mechanism from that responsible for the peak. For momenta below about 2 GeV/c, a flat region appears, possibly from more central collisions. Next lets, examine these data in another manner. In Fig. 12 contours of constant invariant cross section are plotted in the rapidity-transverse momentum (p_T) plane. The dominance of

projectile fragmentation in these data is evident; however, an antistropy is also present. One clearly sees a limitation in longitudinal momentum at large p_T, perhaps indicating a source of protons in the central region (intermediate rapidity).

These data can be used to test the validity of the hypothesis of limiting fragmentation as applied to nuclear collisions at these energies. Limiting fragmentation states[18] that the invariant cross section should become independent of energy, i.e.,

$$\lim_{s\to\infty} E \frac{d^3\sigma^c_{ab}}{dp^3} (s,p_{\parallel},p_T) \to \rho_a(p_{\parallel},p_T) \quad . \tag{4}$$

For alpha fragmentation data the concept can be tested by comparing the transverse momentum distributions at a given proton momentum, chosen here to be protons at beam velocity. This is shown in Fig. 13 for the three different alpha energies and in Fig. 14 on a reduced p_T scale. There is essentially no energy dependence of the invariant cross section, except for the 0.93 GeV/c/nucleon data which is about 10-15 percent lower than the others near $p_T = 0$. By also comparing these distributions in the projectile rest frame, it was concluded that limiting fragmentation was verified for these data to the level of ±7-10 percent out to values of $p_{\parallel}^{PROJ} \sim 0.4$ GeV/c, for 1-2 GeV/nucleon alpha fragmentation to protons. Scaling over this energy range however does not hold. This is demonstrated in Fig. 15, where the cross section vs the Feynman scaling parameter X' is plotted. Clearly, Feynman scaling does not hold at these energies, although the differences of these distributions in the peak for the 1.05 and 2.1 Gev/nucleon data are within a factor of two or three of each other.

As we have just seen, the alpha fragmentation data are rich in structure and possess certain limiting characteristics. One hopes to use this knowledge to obtain information about the reaction mechanisms and ultimately to extract momentum distributions. Thus the goal is to obtain the structure function of the fragmenting nucleus from such measurements. Some success along these lines has been achieved.

In a recent preprint, Fujita and Hufner[19] have analyzed the results[1-2] of $\alpha + C \rightarrow {}^3He + x$. They employ a model in which the ^3He can arise from three distinct processes as schematically shown in Fig. 16. These correspond to:

1. Elastic fragmentation (EF), where the target remains in the ground state.
2. Spectator part (SP), where the neutron is knocked out of the ^4He and interacts with the target.
3. Knock-out (KO), where the ^3He is knocked out of the ^4He and interacts with the target.

The model is calculated in the framework of Glauber theory. Figure 17 shows a comparison between the calculation and the data. Agreement within the region of the fragmentation peak is good and they conclude that this region does indeed reflect in a simple way the momentum distribution of the (^3He,^3H) inside the alpha particle before fragmentation. However, the agreement away from the peak is not as good, and they suggest that this might be evidence for nucleon-nucleon correlations.

Wong and Blankenbecler[20] have analyzed the results[1-2] from the reaction $\alpha + C \rightarrow p + X$ with the aim of extracting nuclear momentum distributions. They have used a model which combines two contributors to the final proton spectrum, as shown in Fig. 18. These include direct fragmentation and hard scattering terms. Comparison with the data is shown in Fig. 19. From their analysis, they are able to extract a semi-empirical nuclear momentum distribution for the alpha particle. They indicate that their extracted distribution also indicates evidence of nuclear correlations and possibly final-state interactions. Thus, as in the previous theoretical study,[19] the posssibility of ground state correlations in nuclei via projectile fragmentation (particularly from the studies in the region of the high momentum tails of the fragmentation distributions) is supported. However, complications with final-state interactions are possible, indicating the need for greater theoretical studies before this becomes a reliable technique for the study of nuclear correlations.

D. More Exclusive Studies of Fragmentation Products: Multi-Particle Final States

By accelerating nuclei to high energies and fragmenting them on light or heavy targets, one opens up new potentials for studying nuclear structure. The use of visual detectors such as bubble or streamer chambers allows the study of charged multi-particle final states. High resolution spectrometers with large detector arrays like HISS[21] (Heavy Ion Spectrometer System) at Berkeley will pioneer a new era in nuclear structure studies by measuring exclusive final states for systems (e.g., $^{12}C \rightarrow 3\alpha$).

Figure 20 demonstrates typical momentum distributions obtained from studying multi-particle final states associated with the fragmentation of light nuclear projectiles. In Fig. 20(a) the momentum distribution for secondaries associated with the break-up of a 8.6 GeV/c ^4He beam in an H_2-bubble chamber experiment[22] displays several peaks. Using projectile fragmentation systematics one can clearly identify these as being due to p (near 2 GeV/c), d (near 4 GeV/c) and t (near 6.5 GeV/c). Figure 20 (b) taken from a streamer chamber study[23] using 320 MeV/nucleon ^{15}N projectiles shows similar peaks. With further analysis one is able to study the dominant reaction channels.

By isolating an exclusive final state (e.g., $^4Hep \rightarrow pp^3H$ or ddp) information on the incident projectile such as the nature and distribution of its constituents can be obtained. For example, Chuvilo et al.[24] have studied the reaction $t + p \rightarrow p + d + n$ at 2 GeV/c using the ITEP 80 cm H_2-bubble chamber. Possible diagrams responsible for this final state are shown in Fig. 21(a). They have performed a calculation based on the incoherent addition of these amplitudes, which require input of N-N parameters and matrix elements for the various dissociation channels of ^3H. Comparison of the model calculation with the data shows agreement with several aspects of the experiment. However, as seen in Fig. 21(b) there is a noticeable discrepancy for the pole model predictions near $\cos\theta^*_{pp} \sim -1$. This could be due to a neglect of final state interactions or possibly to correlations in the incident triton which have not been included in the calculation.

Ruiz et al.[25] have studied the 0^0-fragmentation of relativistic ^6Li using a magnetic spectrometer in association with spark chambers. They find evidence for the dissociation of ^6Li into $^3H + {}^2H + p$ and $^3He + {}^2H + n$, with each of these channels being about 20 percent of the $^6Li \rightarrow {}^4He + {}^2H$ channel. They suggest that the most promising production mechanisms for this are sequential decay through the 16.7 MeV excited states of ^5Li and ^5He and single-nucleon emission by virtual nuclei.

Through the study of multi-particle final states in projectile fragmentation, vital information on the reaction dynamics can be obtained as shown above. This in turn can be used to extract information of considerable interest to the field of nuclear structure.

E. A-A Total Cross Sections, and Mean-Free-Path Measurements

Next, I want to discuss some features of A-A collisions which although not entirely due to peripheral processes, nevertheless can be thought of in that category. I will now describe results on total-cross section measurements and some recent evidence for anomalous nuclei as inferred from reaction mean-free-path measurements of relativistic projectile fragments.

Jaros et al.[26] have measured total cross sections for beams of p, d, α, C on like targets at Berkeley. Glauber multiple scattering theory[27] has been used to accurately predict N-A total cross sections in the few GeV range. The formalism involves folding the basic N-N scattering amplitudes with known nuclear matter distributions. The theory has been extended to A-A collisions,[28] and used to predict total and inelastic cross sections. The theory is essentially geometrical and predicts that, $\sigma_T \propto (A_{tgt}^{1/3} + A_{proj}^{1/3})^2$. The primary purpose of the experiment was to provide data which could be used to test the predictions of the model.

In addition, an observation by Gribov[29] also provided stimulus for this experiment. He noted that if one naively applied Regge factorization to nucleus-nucleus collisions it would lead to a very different A-dependence for σ_T than that expected from geometrical considerations. If one assumes factorization and Pomeron dominance, then we can write that the elastic scattering amplitude, $F_{e\ell} \propto g_{\underline{P}A} g_{\underline{P}B}$, where g's

refer to the appropriate vertex-Pomeron coupling constants for nucleus A colliding with B. Using the optical theorem, which relates the imaginary part of the elastic amplitude to σ_T, one arrives at the relationship:

$$\sigma_T(AA) = \frac{\sigma_T^2(AB)}{\sigma_T^2(BB)} \quad . \tag{5}$$

If we let B = nucleon = p, and use fact that $\sigma_T(pA) \propto A^{2/3}$, we obtain:

$$\sigma_T(AA) \propto A^{4/3} \quad . \tag{6}$$

Thus, factorization predicts $A^{4/3}$, while a Glauber approach would predict $A^{2/3}$, quite different and easily testable.

The "good geometry" transmission technique[30] was used to make these measurements. The technique consists of measuring the beam particles which are scattered by the target with a set of circular counters of increasing size. In this way, one can extrapolate the measurements to zero solid angle. There are two contributions to the scattering process at small angles; Coulomb and nuclear scattering. With nuclear beams and targets, the Coulomb amplitude will necessarily play a larger role. The separation of the Coulomb and nuclear effects are major theoretical and experimental problems.

Figure 22 shows the results of these measurements at 2.1 GeV/nucleon. The solid and dashed curves are the predictions of Glauber theory and the factorization relation, respectively. The data is seen to be in excellent agreement with the Glauber prediction for all data points except the CC point which lies slightly below the Glauber theory prediction. The fact that the factorization prediction is not satisfied could be anticipated, since it is only supposed to be valid at energies much larger than those available in this experiment.

Streamer chamber studies at Dubna[32] have extended measurements of inelastic A-A cross sections for carbon beams up to 4.5 GeV/c/nucleon. Results of this work along with others is shown in Fig. 23. The results displayed as $(\sigma_{inel})^{1/2}$ vs $(A_{tgt}^{1/3} + A_{proj}^{1/3})$ clearly demonstrate the geometric inter-

pretation to these cross sections at energies of a few GeV/nucleon.

Next, I want to consider some very recent results on the reaction mean-free-path (mfp) of projectile fragments. Since about 1954 there have been a number of experiments with high energy cosmic-ray heavy-ions that have reported anomolously short mfp measurements associated with the fragmentation products.

In order to study this effect with higher statistics, a joint LBL/NRC/Marburg collaboration[32] has exposed a series of emulsion stacks to ~2 GeV/nucleon ^{16}O and ^{56}Fe beams from the Bevalac. To obtain their mfp's they follow projectile fragments from an initial interaction in the emulsion, through successive generations (as high as 7th observed) of collisions. They have obtained a sample of 1460 events from their scan. They conclude that there is a significant sample (~6 percent) of projectile fragments which exhibit an anomalously short mfp for the first few centimeters after an interaction. At larger distances these fragments exhibit a more "normal" mfp. Figure 24 shows this feature, where D is the distance (cm) from a primary interaction vertex. The dashed line is what would be expected if there were no anomalously short mfp nuclei, and the solid line refers to an admixture of the anomalous nuclei. Note also that the vertical axis has a suppressed zero. The solid points are the data summed over both ^{16}O and ^{56}Fe events as well as averaging over the outgoing fragment charges ($3 \leq Z \leq 26$). The scatter in the data points provides a measure of the associated uncertainties (primarily statistical). This is clearly a very intruiging result which must be examined with additional experiments.[33] The level of statistics needs to be improved and systematics (dependence on beam, energy, fragment type, etc.) of the effect need closer scrutiny. At present, one needs to be very cautious and critical about this result, but if it holds up it could signal the existence of a new and interesting nuclear phenomena.

TARGET FRAGMENTATION

We have up to this point been discussing the fragmentation process from the vantage point of the projectile. There, as we have seen the fragments are typically emitted at high energies and in the forward direction. In this regime, the techniques of high energy are most suitable.

Now we want to transform to the target frame and investigate reaction products emitted in N-A and A-A collisions. At high energies, where the rapidity interval between projectile and target are well separated, the physics of the two fragmentation regions must be similar. However, the experimental techniques are often considerably different. The projectile fragmentation peaks which appear near the projectile velocity, when transformed to the target frame correspond to near zero energy fragments. An example of a target fragmentation process can be seen by studying low energy protons ($T_p^{LAB} < 200$ MeV) at large production angles. Figure 25 shows the proton spectrum at $\theta_{LAB} = 150^o$ in p + U collisions at 1.04 GeV. The data[34] can be simply parameterized as the incoherent sum of two Gaussians. The lower Gaussian ($\sigma_1 = 80$ MeV/c) corresponding to the primary proton fragmentation peak we would expect to see if we fragmented a U-beam on a proton target (i.e., U + p → p + X). The second Gaussian provides the high energy behavior of this distribution and is similar in nature to the high energy tail that was discussed earlier for alpha particle fragmentation (see Fig. 11 for example). We will discuss this further in connection with nuclear correlations obtained from proton production at 180°.

The discussion on target fragmentation will be restricted to high energy particle production at backward angles. Here, the area of interest will be particles produced at energies well beyond those expected from simple N-N collisions.

A. High Energy Proton Production at 180°

The production of high energy backward protons has received considerable experimental and theoretical attention. Frankel and collaborators have studied this process in p-A collisions at 0.6 and 0.8 GeV[35] and most recently at 400 GeV at FNAL.[36] Frankel[37] has interpreted the lower energy data in terms of a model (quasi-two-body-scaling) in which the primary mechanism for backward proton production is a scattering between the incident proton and a target nucleon. It is the target nucleon which is boosted onto the mass-shell and appears in the backward direction. He was able to show that for the 0.6 and 0.8 GeV data a simple structure function ($G(k_{min}) \sim e^{-k/k_0}$) is able to

reproduce the data, and suggested that this structure function was a measure of the internal momentum distribution of nucleons inside the target. Remember that backward protons are strictly forbidden in free N-N collisions. Thus, one hopes that backward proton production can provide us with a tool for extracting information on nuclear momentum distributions. However, a word of caution! Gottfried[38] had earlier pointed out the difficulties associated with extracting information on high internal momentum components due to mean field effects. Amado and Woloshyn[39] have demonstrated that final state interactions preclude a simple interpretation of the backward momenta in (p,p') reactions.[37] However, the study of high momentum protons can provide valuable information on the production mechanisms, and possibly on internal momentum distributions.

Our group at Berkeley[3] has concluded a systematic study of the inclusive spectrum of energetic protons ($0.4 \leq p \leq 1.0$ GeV/c) emitted at 180° using the full range of energies and projectiles available at the Bevalac. Earlier measurements[40] at laboratory angles 120° using high energy ν, γ, π and p beams have shown that the spectra of protons above 400 MeV/c is independent of projectile type and energy. This strongly suggests that such experiments do indeed probe fundamental characteristics of the ground state of the target nucleus.

The energy dependence of the cross sections is shown in Fig. 26 along with results of other experiments.[35,36,41,42] A limiting behavior of these distributions sets in above energies of 1-2 GeV/nucleon. A slight rise is seen in the 400 GeV data measured at 160°. The spectrum at 90 MeV has an elastic kinematic limit at 392 MeV/c. The lack of dependence on incident energy is exhibited for all targets and suggests that limiting target fragmentation[18] appears to set in around 2 GeV.

Figure 27 shows the dependence on projectile mass for a carbon target. The shapes are seen to be roughly independent of projectile mass. Plotted in the same figure (in the projectile rest frame) are data from Papp[43] for $C + C \rightarrow p(2.5^{\circ}) + X$. The break found in the combined $C + C \rightarrow p + x$ data near 350 MeV/c is similar to that found in extracted momentum distributions from (γ,p) experiments. Recent theoretical investigations[44-46] show that the internal momentum distributions in nuclei can be approximated by two overlapping Gaussians when short range

correlations are included. The low momentum Gaussian is dominated by single-particle characteristics of the momentum distributions and the second Gaussian emerges when short range correlations are considered. The solid line is a double Gaussian parameterization of the C + C → p data. If the internal momentum distributions are indeed correctly specified by the models, then one is led to conjecture that the shapes of the measured distributions in the momentum region $0.4 \leq p \leq 1.0$ GeV/c are a consequence of the presence of nuclear correlations. Note also that the wide angle proton data of Fig. 25 displays this same double-Gaussian shape.

To further study the dependence of these cross sections on projectile and target mass and energy, we have parameterized our data in the momentum range $0.4 \leq p \leq 1.0$ GeV/c in the form $d\sigma/dp^3 = \sigma_T/(\sqrt{2\pi})^3\alpha^3) \times e^{-(p^2/2\alpha^2)}$ (where $\sigma_T = \int(d\sigma/dp^3)\, d^3p$). The fits are good for incident kinetic energies $T \geq 1.05$ GeV/nucleon having typical uncertainties of ±5 MeV/c for α and ±10 percent for σ_T. The dependence of α on the target and projectile masses is shown in Fig. 28(a). The mass dependences are relatively weak. The dependence on incident energy is more dramatic and the limiting nature of the cross sections is reflected in this dependence. A limiting value of 220 ±10 MeV/c is indicated by data at various backward angles and energies above 5 GeV. The dependence of σ_T on the masses at 1.05 GeV/nucleon incident energy is shown in Fig. 28(b). An approximate $A_p^{2/3}A_t^{4/3}$ (p = proj, t = tgt) dependence is found for σ_T at 1.05 GeV/nucleon and 2.1 GeV/nucleon. The A_p dependence is expected in a limiting fragmentation model[47] where the projectile is seen as a contracted disk by the target nucleus. In such a model, one could interpret the measured momenta as reflecting information of the target. The A_t dependence argues against incoherent collisions and indicates the involvement of more than one target nucleon in backward nucleon production. Inclusive proton data in the fragmentation region from p + d and p + α reactions[1,48] show a similar break in the distributions at about 300 MeV/c. This would argue against a multiple scattering cascade as the dominant mechanism, at least for light nuclei. Definitive theoretical work on the contributions of multiple scattering is, however, still necessary to justify this conclusion.

Thus, there now appears to be a body of information developing from single particle spectra indicating that high momentum protons at backward angles are manifestations of correlations in the ground state of nuclei. Indeed, there has recently been several models which incorporate nucleon correlations to explain these data. A model by Fujita and Hufner[49] includes both initial correlations between nucleons in the target and final correlations between two nucleons. The final state interaction with the rest of the A-2 nucleons is being neglected. Fujita has extended this model to include multiple correlations.[50] The improved model describes well the incident energy dependence of backward proton spectra in the region $0.4 \leq p \leq 1.0$ GeV/c for the intermediate energy range 0.6 to 1.0 GeV. Theoretical work by Frankfurt and Strikman[51] and Yukawa and Furui[52] indicate that backward spectra induced by high energy probes are mainly composed of spectator nucleons from the breakup of correlated pairs in the nucleus. As such, these backward nucleons potentially reflect direct information of the nuclear wavefunction.

B. Pion Production at 180° in A-A Collisions

Let us now turn to the production of pions at 180°. A principle reason for studying production of energetic pions from nuclei in the backward direction is that in free N-N collisions such production is kinematically restricted. Observation of pions beyond this kinematic limit may then be evidence for exotic production mechanisms such as production from clusters.[51,53-55] Early experiments by Baldin et al.[56] using 5.14 and 7.52 GeV protons observed charged pions at 180° with energies up to four times larger than expected from free N-N collisions. They argued that simple Fermi motion could not account for this effect and stated that the dominant mechanism for producing such pions was an interaction between the incident proton and multi-nucleon clusters in the target, referring to this mechanism as cumulative production. A recent experiment[57] using 0.6 GeV protons measured pions at 155° and concluded that the dominant mechanism was single scattering ($NN \rightarrow NN\pi$). A question we wished to answer was whether there are two different mechanisms, one dominating below ~1 GeV and the other above ~5 GeV; and if so, how is the transition between them made. Also the Dubna

experiment[56] observed that the pion spectra were exponential with a slope parameter $T_0 \sim 60$ MeV, independent of energy. So that we wanted to obtain data below 5 GeV to see where this trend breaks down. Finally, we wanted to test the hard-scattering model of Schmidt and Blankenbecler[58] which had been successful in reproducing trends observed in high energy forward pion production experiments.

We now turn to the results from our recent measurements of pion production at 180° in A-A collisions. We have measured the following:

$$A_1 + A_2 \rightarrow \pi^{\pm}(180^{\circ}) + x \quad ,$$

where A_1 = p,α,C,Ar and A_2 = C,Al,Cu,Sn,Pb. Incident energies were 0.8-4.89 GeV for protons, 1.05 and 2.1 GeV/nucleon for alphas and carbon, and 1.05 and 1.8 GeV/nucleon for Ar.

First, let us consider results on $\pi^{\pm}$ production by protons.[59] The pion spectra were all found to be exponential in character, with the slope parameter T_0 being weakly dependent on target mass. Figure 29 shows the dependence on energy of the slope parameter T_0 and the ratio $R = \pi^-/\pi^+$ for a Cu target. Both are observed to rise with energy until about 3-4 GeV, after which a leveling off occurs. The dashed curve represents the predictions of an "effective target" model[55] where the incident proton is assumed to interact and excite in a collective fashion the row of nucleons along its path. In de-exciting pions are emitted, much as in thermal models. Although the model agrees nicely with the energy dependence of T_0, it does not reproduce the magnitude of the cross sections, being low by a factor of 4 at the lower energies. Since the model does not distinguish between positive and negative pions, it is in disagreement with the π^-/π^+ ratio.

The trends observed in Fig. 29 are common to all targets. Above about 3-4 GeV, a limiting value is reached. Cross sections for multi-pion production in N-N collisions are increasing in this region, and could be associated with these limiting features. Detailed calculations, including absorption and charge-exchange effects are needed to ascertain fully the contributions of single-scattering processes in this energy region.

Figure 30 demonstrates the dependence on target mass in this energy region. The cross sections were parameterized as $\sigma_{inv} \propto A^n$. K > 1 corresponds to the cummulative production region.[56] The variations observed in the A-dependence between 0.8 and 4.89 GeV suggest the possibility that different mechanisms are responsible for pion production over this energy region with a smooth evolution from one to the other as the energy is increased. Fredriksson[60] has recently analyzed this A-dependence within the scope of the coherent tube and fluctuon models. The comparison is shown in Fig. 31. He concludes that the data support a model in which the proton interacts collectively with all matter within 1 fm in its rest frame at the time of collision.

Finally, our 180° production data provide a definitive test of the hard-scattering model of Schmidt and Blankenbecker.[58] This model, which successfully fit the forward pion production data of Papp et al.,[61] predicts that the 180° negative pion spectrum should be independent of energy, depending only on the scaling parameter x' in the form $(1-x')^N$. Simple counting arguments yield N = 6A-5, so that for a Cu target (A = 63) we expect $\sigma_{inv} \propto (1-x')^{373}$. Figure 32 shows a plot of the invariant cross-section vs. x'. Lack of scaling is evident. However, each spectrum can be represented as $(1-x')^N$, but for values of N much small than predicted (see solid lines through data). Landau and Gyulassy[62] have recently modified this model by assuming that the nucleon interacts with a nucleon cluster, rather than the entire nucleus. Agreement with the trend of the data is found. The individual clusters are assumed to have internal motion, an exponential distribution providing the best results. They are able to reproduce the data using clusters of one to four nucleons, but with no single choice being preferred.

Wong and Blankenbecker[63] have generalized the Feynman scaling variable to massive but weakly bound systems like nuclei, for both proton and pion production. For pion production, they invoke the hardscattering mechanism schematically shown in Fig. 18(b). The Dubna[56] and Berkeley[59] results on 180° pion production are compared with this new scaling variable X_H in Fig. 33. The data, spanning the energy range from 0.8-7.51 GeV, do appear to fall on a single curve of the form

$(1-X_H)$[88]; whereas the model predicts $(1-X_H)$.[68] It should also be noted that there is a considerable spread of the data about a single curve. At the present time, the scaling parameter X_H is a somewhat complicated function which does not easily yield to physical interpretation. However, if this new approach holds up, it contains the promise of yielding valuable information on nuclear structure functions.

We have also studied the production of charged pions at 180° with energetic beams of alphas, carbon and argon nuclei. These data are still in a preliminary stage of analysis, but some of the early systematics for the heavier beams are outlined below:

1) The pion spectra continue to behave approximately in an exponential fashion, with slope parameters 3-5 MeV larger than the case of proton beams.
2) The ratio, $R = \pi^-/\pi^+$, for the integrated pion yields from a Cu target is ~1 for the carbon beam, and 1.15 for an argon beam. The increase above R=1 for the argon beam presumably reflects the increased number of neutrons over protons which would favor π^+ production.
3) The dependence of the integrated pion yields on target (A_t) and projectile (A_p) is found to be, $\sigma \propto (A_p A_t)^{0.8}$.

C. Backward Particle Production-Streamer Chamber Studies

In order to obtain more information on the mechanisms responsible for high energy backward particle production we have supplemented our 180° measurements with a 2.1 GeV proton bombardment of various targets (C, KCl, BaI_2) located inside the Berkeley streamer chamber.[23,64] The streamer chamber offers the following advantages:

1) 4π geometry.
2) Large efficiency for charged multi-particle final states.
3) Capability of being selectively triggered.

We triggered the chamber on any backward particle ($\theta_{LAB} > 90^o$). The resulting film has been scanned and measured. A sample event, obtained from the computer reconstruction of the measured tracks is shown in Fig. 34. Although the analysis is at an

early stage, there are interesting features that can be reported at this time. First, a large fraction of the events (~50 percent) are found to have an associated negative track which can be identified as a pion. Typically this pion appears at $\theta_{LAB} < 90°$. Thus, backward particle emission (typically the backward track is a proton) at 2.1 GeV is often accompanied by the production of a pion. This suggests that the simple quasi-elastic process, NN→NN, as suggested by Frankel,[37] is not the dominant mechanism at this energy for producing backward protons.

Further information on possible reaction mechanisms can be obtained from a rapidity plot of the positively-charged particles (mostly protons) of these events. This is shown in Fig. 35. Several features are evident:

1) Most of the events are centered about the target rapidity, i.e., target fragmentation dominates.
2) Some contribution from quasi-elastic processes is evident (near beam rapidity).
3) Large number of events with high p_T.

Results for C and KCl targets are similar, except for an increase of the number of forward events as target mass decreases; probably due to a decrease in multiple scattering processes.

There appears to be evidence for the role of pion production followed by absorption in the nuclear environment in the ejection of high energy backward protons.[65] There are two possibilities here:

(a) Production of a pion followed by absorption of the pion on two target nucleons resulting in two back-to-back nucleons, and
(b) production of the $\Delta^{++}(1232)$ and its subsequent absorption on a target nucleon via, $\Delta + N \rightarrow N + N$, resulting in the emission of two protons which will tend to have a near 180^0 correlation.

A preliminary study of the correlation of a backward positive track (most likely a proton) and any other positive track shows a correlation function which peaks for 180°. Figure 36 shows the laboratory correlation for pairs of positive particles as a function of the cosine of the angle between the two particles (one of the pair is always emitted into the backward hemisphere). A strong correlation at 180^0 is observed. This correlation is

enhanced if a momentum cut p > 300 MeV/c is introduced. This effect does not appear to be explained by phase space arguments. Figure 37 shows the correlation for 4 and 5-prong events, along with the predictions of three phase space calculations, which do not exhibit a strong 180^{0} correlation. Thus, although a pion does not necessarily appear in the final state as such, its creation does appear to play a key role as a production mechanism for backward protons. Further studies are continuing with these new streamer chamber data to understand the mechanisms responsible for particle production at backward angles.

CONCLUDING REMARKS

The study of projectile and target fragmentation processes gives every indication of being a rich source of information on nuclear structure. There is an accumulation of information indicating that both single-particle momentum distributions and higher order correlations (whether they are called high momentum components or multi-nucleon clusters) play an important role in particle production in the regions kinematically forbidden to free N-N collisions. Whether one can extract this information in a clean fashion from the complications of final state interactions is still a topic of considerable uncertainty. Single-particle inclusive studies have taken us as far as they can in these studies, and two-particle and possibly higher level correlations need to be undertaken.

Projectile fragmentation at high energies has proven to be a powerful ally in the production of new exotic nuclei. In the future, secondary beams are possible, which will allow even more detailed information to be obtained. The area of cosmic-rays and astrophysics continues to be aided through measurements of various fragmentation cross sections. In terms of high energy physics ideas, we see that at energies of ~1-2 GeV/nucleon limiting distributions are appearing. In some sense, for nuclei at a few GeV/nucleon, we are in an apparent asymptotic region, with its accompanying simplifications.

In 1982, much heavier beams (up to uranium) will be available at Berkeley. These beams will possess very large Z-values, which will upgrade the role the Coulomb field plays in these collisions. Whether this will present new exciting avenues of

research is not known at present, but it will certainly be an experimental challenge.

ACKNOWLEDGMENTS

I would like to thank my colleagues at Berkeley, with whom I have had many productive discussions on Bevalac physics; particularly, J. Geaga, J. Harris, S. Chessin, D. Hendrie, R. Treuhaft, A. Sandoval, S. Nagamiya and M. Gyulassy. I also wish to thank Professor S. Homma for inviting me to speak at the Summer Study.

REFERENCES

1. L. M. Anderson, Ph. D. Thesis, September 1977, LBL-6769, not published.
2. L. M. Anderson, O. Chamberlain, S. Nagamiya, S. Nissen-Meyer, D. Nygren, L. Schroeder, G. Shapiro and H. Steiner, LBL-9493 (July 1979).
3. J. V. Geaga, S. A. Chessin, J. Y. Grossiord, J. W. Harris, D. L. Hendrie, L. S. Schroeder, R. N. Treuhaft and K. Van Bibber, LBL-10265 (1980), submitted to Phys., Rev. Lett.
4. See talk by H. Gutbrod in the Proceedings of this summer study.
5. See talk by A. Goldhaber in the Proceedings of this summer study.
6. D. E. Greiner, P. J. Lindstrom, H. H. Heckman, B. Cork, and F. S. Bieser, Phys. Rev. Lett. 35, 152 (1975), and H. H. Heckman, D. E. Greiner, P. J. Lindstrom, and F. S. Bieser, Phys. Rev. Lett 28, 926 (1976).
7. A. S. Goldhaber, Phys. Lett. 53B, 306 (1974).
8. H. Feshbach and K. Huang, Phys. Lett. 47B, 300 (1973).
9. J. D. Bowman, W. J. Swiatecki and C. F. Tsang, unpublished LBL report (1973).
10. J. Hufner, K. Schafer and B. Shurman, Phys. Rev. C12, 1888 (1975).
11. Y. Abul-Magd and J. Hufner, Nucl. Phys. A308, 419 (1978).
12. D. K. Scott, M. Bini, P. Doll, C. K. Gelbke, D. L. Hendrie, J. L. Laville, J. Mahoney, A. Menchaca-Rocha, M. C. Mermaz, C. Olmer, T. J. M. Symons, X. P. Viyogi, K. Van Bibber, H. Weiman, P. J. Siemens, LBL-7729 (1979).

13. K. Van Bibber, D. L. Hendrie, D. K. Scott, H. H. Weiman, L. S. Schroeder, J. V. Geaga, S. A. Chessin, R. Treuhaft, J. Y. Grossiord, J. O. Rassmussen and C. Y. Wong, Phys. Rev. Lett. 43, 840 (1979).
14. D. K. Scott, Towards Relativistic Heavy Ion Collisions-By Small Steps Towards the Stars, a series of lectures given at the International School of Nuclear Physics, "Ettore Majorana" Center for Scientific Culture, Erice, Sicily, March 26-April 6, 1979, LBL-8931 (1979).
15. G. D. Westfall, T. J. M. Symons, D. E. Greiner, H. H. Heckman, P. J. Lindstrom, J. Mahoney, A. C. Shotter, D. K. Scott, H. J. Crawford, C. McParland, T. C. Awes, C. K. Gelbke and J. M. Kidd, Phys. Rev. Lett. 43, 1859 (1979).
16. H. Crawford, R. LeGrain, P. Lindstrom, M. J. Murphy, T. J. M. Symons and G. Westfall, Expt. 561H at the Berkeley Bevalac Facility.
17. B. Berman, D. Greiner, F. Bieser, B. Cork, H. Crawford, H. Heckman and P. Lindstrom, E350H at the Berkeley Bevalac Facility.
18. W. R. Frazer, I. Ingber, C. H. Mehta, C. M. Poon, D. Silverman, K. Stowe, P. D. Ting and H. Y. Yesian, Rev. Mod. Phys. 44, 284 (1972).
19. T. Fujita and J. Hufner, Univ. of Heidelberg (Max Planck Institute) preprint (1979). Submitted to Nucl. Phys. A.
20. C. Y. Wong and R. Blankenbecler, pg. 105 of the Proceedings of the Workshop on Nuclear Dynamics, March 17-21, 1980, Granlibakken, Tahoe City, California, LBL-10688.
21. HISS consists of a large superconducting magnet which will have the capability of fields up to ~35 Kgauss. Detector arrays will be used in conjunction with particle identification elements and the large magnetic volume to investigate a wide range of nuclear reactions from peripheral to central collisions. Operation of this system is planned for early 1981.
22. V. V. Glagolev et al., JINR (Dubna) preprint E1-12943 (1979).
23. L. S. Schroeder, Nucl. Inst. and Meth. 162, 385 (1979).
24. I. V. Chuvilo, V. A. Ergabov, V. E. Grechko, Yu, V. Korolev, Ya. M. Selektor, V. V. Solovjev, V. N. Shulyachenko, Yu. V. Trebukhovsky, V. F. Turov, I. A. Vanyushin, I. D. Voytenko and S. M. Zombkovsky, Phys. Lett. 91B, 349 (1980).

25. C. L. Ruiz, R. W. Huggett and P. N. Kirk, Phys. Rev. Lett 43, 334 (1979); and C. L. Ruiz, P. N. Kirk and R. W. Huggett, LSU preprint (1980), submitted to Phys. Rev. Lett. for publication.
26. J. Jaros, A. Wagner, L. Anderson, O. Chamberlain, R. Z. Fuzesy, J. Gallup, W. Gorn, L. Schroeder, S. Shannon, G. Shapira and H. Steiner, Phys. Rev. C18, 2273 (1978).
27. R. J. Glauber in Lectures in Theoretical Physics, Vol. 1 (Interscience, New York, 1959), pg. 315, R. J. Glauber in High Energy Physics and Nuclear Structure (North-Holland, Amsterdam, 1967), pg. 311, and R. J. Glauber in High Energy Physics and Nuclear Science (North-Holland, Amsterdam, 1979), pg. 207.
28. W. Czyz and L. C. Maximon, Annals of Physics 52, 59 (1969).
29. V. N. Gribov, Sov. Jour, Nucl. Phys. 9, 369 (1969).
30. G. Giacomelli in Progress in Nuclear Physics, Vol. 12 (Pergamon Press, New York, 1979), pg. 77.
31. J. Bartke, in Proceedings of the 8th International Conference on High Energy Physics and Nuclear Structure, Vancouver, August (1979), D. F. Measday and A. W. Thomas (eds.), North Holland; and published in Nucl. Phys. A335, 481 (1980).
32. E. M. Friedlander, R. W. Gimpel, H. H. Heckman, Y. J. Karant, B. Judek and E. Ganssauge, LBL preprint (June 1980).
33. The LBL/NRC/Marburg group will be exposing more emulsion stacks to a wider variety of beams to increase statistics and study the systematics of this effect (Expt. 559H at the Bevalac).
34. A. Sandoval, private communication (1980).
35. S. Frankel, W. Frati, O. Van Dyck, R. Werbeck and V. Highland, Phys. Rev. Lett. 36, 642 (1976); S. Frankel, W. Frati, G. Blanpied, G. W. Hoffmann, T. Kozlowski, C. Morris, H. A. Thiessen, O. Van Dyck, R. Ridge and C. Whitten, Phys. Rev. C18, 1375 (1978).
36. Y. D. Bayukov, V. I. Efremenko, S. Frankel, W. Frati, M. Gazzaly, G. A. Leskin, N. A. Nikiforov, C. F. Perdrisat, V. I. Tchistilin and y. M. Zaitsev, Phys. Rev. C20, 764 (1979).
37. S. Frankel, Phys. Rev. Lett. 38, 1338 (1977).
38. K. Gottfried, Ann. Phys. 21, 29 (1973).
39. R. D. Amado and R. M. Woloshyn, Phys. Lett. 69B, 400 (1977).

40. G. A. Leskin, International Conference on High Energy Physics, ITEP-147 (1976) and references therein.
41. J. R. Wu, C. C. Chang and H. H. Holmgren, Phys. Rev. C19, 698 (1979).
42. A. M. Baldin, preprint JINR-P1-11302, Dubna (1978).
43. J. Papp, LBL-3633, Berkeley (1975), Ph. D. Thesis (unpublished).
44. J. G. Zabolitsky and W. Ey, Phys. Lett. 76B, 527 (1978).
45. O. Bohigas and S. Stringari, Orsay preprint IPNO/TH 79-59 (1979).
46. J. W. Van Orden et al., University of Maryland, TR 80-046 (1979).
47. M. L. Perl, High Energy Hadron Physics, John Wiley and Sons, New York, pg. 201 (1974).
48. A. M. Baldin et al., preprint JINR-P1-11168, Dubna (1977).
49. T. Fujita and J. Hufner, Nucl. Phys. A314, 317 (1979).
50. T. Fujita, Nucl. Phys. A324, 409 (1979).
51. L. L. Frankfurt and M. I. Strikman, Phys. lett. 83B, 497 (1979).
52. T. Yukawa and S. Furui, Phys. Rev. C20, 2316 (1979).
53. V. V. Burov, V. K. Lukyanov and A. I. Titov, Phys. Lett. 67B, 46 (1977).
54. M. I. Gorenstein and G. M. Zinovjev, Phys. Lett. 67B, 100 (1977).
55. H. B. Mathis and Meng Ta-Chung, Phys. Rev. C18, 952 (1978).
56. A. M. Baldin, N. Giordenescu, V. N. Zubarev, L. K. Ivanova, N. S. Moroz, A. A. Povtoreiko, V. B. Radomanov and V. S. Stavinskii, Yad. Fiz. 20, 1201 (1975) [Sov. J. Nucl. Phys. 29, 629 (1976)].
57. C. F. Perdrisat, S. Frankel and W. Frati, Phys. Rev. C18, 1764 (1978).
58. I. A. Schmidt and R. Blankenbecler, Phys. Rev. D15, 3321 (1977).
59. L. S. Schroeder, S. A. Chessin, J. V. Geaga, J. Y. Grossiord, J. W. Harris, D. L. Hendrie, R. Treuhaft and K. Van Bibber, Phys. Rev. Lett. 43, 1787 (1979).
60. S. Fredriksson, Royal Inst. of Tech. preprint TRITA-TFY-80-6 (Stockholm-1980).
61. J. Papp, J. Jaros, L. Schroeder, J. Staples, H. Steiner, A. Wagner and J. Wiss, Phys. Rev. Lett. 34, 601 (1975).

62. R. M. Landau and M. Guylassy, Phys. Rev. C19, 149 (1979).
63. C. Y. Wong and R. Blankenbecler, pg. 109 of the Proceedings of the Workshop on Nuclear Dynamics, March 17-21, 1980 Granlibakken, Tahoe City, California, LBL-10688.
64. LBL/GSI Streamer Chamber Collaboration: J. W. Harris, J. Brannigan, J. V. Geaga, L. S. Schroeder, R. N. Treuhaft, A. Sandoval, H. E. Stelzer and R. Stock (Experiment 400M at the Bevalac).
65. J. W. Harris, pg. 80 in the Proceedings of the Workshop on Nuclear Dynamics, March 17-21, 1980, Ganlibakken, Tahoe City, California.

FIGURE CAPTIONS

Fig. 1. Data for the reaction $\alpha + Cu \rightarrow p(0,180^0) + x$ at 2.1 GeV/nucleon. Data at 0^0 is from Ref. 1 and at 180^0 from Ref. 3. The invariant cross-section is plotted against Lab momentum (GeV/c).

Fig. 2. (a) Interaction of 0.8 GeV/nucleon ^{12}C projectile with target located inside the steamer chamber. Positive particles are bent downward in the magnetic field of the chamber. (b) Interaction of a 1.8 GeV/nucleon ^{40}Ar with Pb_3O_4 target located inside the streamer chamber leading to multi-particle final state. Tracks bending upward are negative pions.

Fig. 3. Data of Ref. 6 showing the fragmentation of an ^{16}O beam at 2.1 GeV/nucleon into carbon isotopes. Cross section (arbitary units) vs momentum/unit charge (rigidity).

Fig. 4. Data of Ref. 6 on the fragmentation process ^{12}C + target $\rightarrow$ ^{10}Be + X at 2.1 GeV/nucleon. Cross section vs longitudinal momentum in the projectile rest frame.

Fig. 5. Target averageo width, $\sigma_{p_{\parallel}}$, of the projectile frame longitudinal momentum distribution (MeV/c) vs observed fragment mass. Data of Ref. 6 for a 2.1 GeV/nucleon ^{16}O beam.

Fig. 6. Data of Ref. 12 for ^{16}O fragmentation into ^{12}C at projectile energies below 20 MeV/nucleon.

Fig. 7. Momentum widths obtained from Gaussian parameterization of projectile fragmentation data as a function of projectile energy. Dashed curve is explained in text.

Fig. 8. Table of isotopes for light nuclei.

Fig. 9. Mass histograms for elements observed in the fragmentation of 212 MeV/nucleon ^{48}Ca by a Be target.

Fig. 10. Target factor γ_T vs target mass. Data are for single-nucleon removal reactions using ^{16}O and ^{12}C beams at 1.05 and 2.1 GeV/nucleon.

Fig. 11. Lorentz invariant cross section for $\alpha + C \rightarrow p + x$ at 2.1 GeV/nucleon as function of the laboratory momentum of the proton. Data are from Refs. 1 and 2.

Fig. 12. Contours of constant invariant cross section in the rapidity-p_T plane. Data for $\alpha + C \rightarrow p + x$ at 2.1 GeV/nucleon from Refs. 1-2.

Fig. 13. Invariant cross section vs p_T for 0.4, 105 and 2.1 GeV/nucleon alphas.

Fig. 14. Invariant cross section vs p_T for 0.4, 105 and 2.1 GeV/nucleon alphas for $p_T < 0.2$ GeV/c.

Fig. 15. Invariant cross section vs $X' = (p_L^{CM}/(p_L^{CM})_{max})$ for alpha fragmentation data of Refs. 1-2.

Fig. 16. Representation of the processes contributing to $\alpha + A \rightarrow {}^3He + x$ calculated by Refs. 19.

Fig. 17. Comparison of the model calculation (Ref. 19) with $\alpha + C \rightarrow ({}^3He, {}^3H) + x$ data (Ref. 1-2). The contributions of the various terms are indicated.

Fig. 18. Diagrams of the two dominant processes contributing to alpha fragmentation to a proton.

Fig. 19. Comparison of model calculation (Ref. 20) with $\alpha + C \rightarrow p + x$ data (Refs. 1-2). Invariant cross section vs (a) Feynman scaling parameter, X_F and (b) transverse momentum of the proton.

Fig. 20. (a) Momentum distribution of secondary charged particles for 3394 3-prong events from 8.56 GeV/c ${}^4He$-p interactions. (b) Rigidity (p/z) distribution for fragments arising from 4- and 6-prong events in 320 MeV/nucleon ${}^{15}N + Pb_3O_4$ interactions.

Fig. 21. (a) Possible contributing diagrams for $t + p \rightarrow pdn$ at 2.5 GeV/c. (b) The $\cos\theta^*_{pp}$ distribution (Ref. 24), where θ^*_{pp} is the angle between the initial and secondary protons in the pn rest system.

Fig. 22. Measured total cross sections ($\sigma_T(AA)$) compared with predictions of factorization and Glauber models. Data of Ref. 26 at 2.1 GeV/nucleon.

Fig. 23. Dependence of the inelastic ${}^{12}C$-nucleus cross section on target mass (A_T).

Fig. 24. Estimated values of the parameter Λ at different distances D from the origin of the projectile fragments. See text for explanation of solid and dashed lines.

Fig. 25. Cross-section ($d^3\sigma/dp^3$) for $p + U \rightarrow p(150^0) + x$ vs momentum of emitted proton.

Fig. 26. Dependence of backward proton inclusive spectra as a function of incident energy.

Fig. 27. Proton inclusive distributions for different projectiles at 1.05 GeV/nucleon.

Fig. 28. (a) Energy (♦), target (o) and projectile (□) dependence of parameter α where A denotes both A_p and A_t. (b) Plot of parameter σ_T vs $A_p^{2/3}A_t^{4/3}$, solid line shows trend expected if dependence is $A_p^{2/3}A_t$.

Fig. 29. Energy dependence of (a) to parameter for pions, and (b) the π^-/π^+ ratio at 180° obtained by integrating each spectra up to 100 MeV from 0.8-4.89 GeV (Ref. 59). The dashed curve in both cases refers to the predictions of the "effective-target model (Ref. 55).

Fig. 30. A-dependence for charged-pion production. Data were fitted by the form A^n; the exponent or is plotted vs the ratio K for (a) 0.8 and 1.05 GeV, (b) 2.1 GeV, and (c) 4.89 GeV protons.

Fig. 31. Comparison of model calculations for A-dependence with the data of Ref. 59.

Fig. 32. Lorentz-invariant cross section vs x' for π^- production at 180° by 0.8, 1.05, 2.1 and 4.89 GeV protons and π^+ production at 180° by 3.5 GeV protons from a Cu target.

Fig. 33. Invariant cross section for $p + Cu \rightarrow \pi^{\pm}(180^o) + X$ vs scaling variable x_H (Ref. 63).

Fig. 34. Typical event obtained by triggering on backward particle, 2.1 GeV p + C interaction.

Fig. 35. Rapidity plot of positive charged-particles from the $p + BaI_2$ reaction at 2.1 GeV. The kinematic limit of elastic scattering in the N-N system is shown by the solid curve.

Fig. 36. Correlation between pairs of positive charged-particles in each event vs cosine of angle between the particles. For each combination, one of the particles is emitted at $\theta_{LAB} > 90^o$. Cuts on particle momentum are indicated.

Fig. 37. Correlation analysis (as in Fig. 36) for all 4 and 5-prong events. Pure phase space calculations for three possible final states are shown.

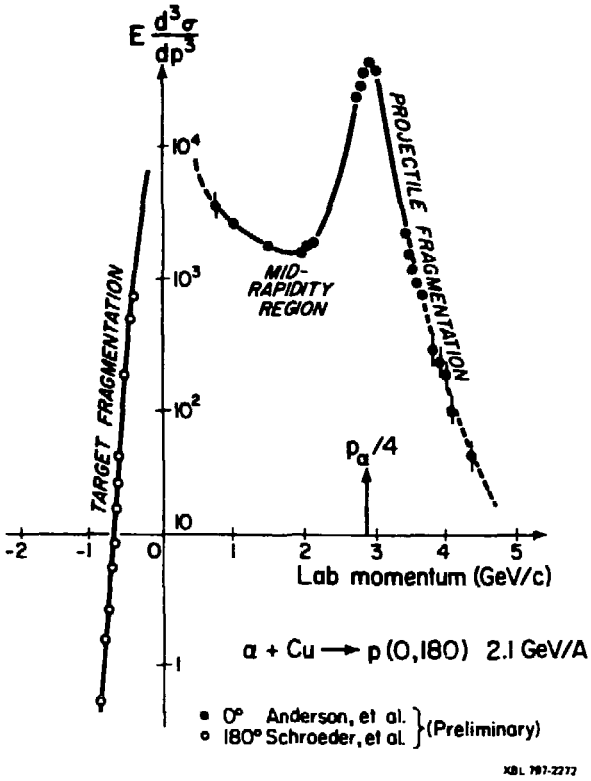
E d³σ/dp³
10⁴
10³
10²
10
1
TARGET FRAGMENTATION
MID-RAPIDITY REGION
PROJECTILE FRAGMENTATION
pα/4
-2
-1
0
1
2
3
4
5
Lab momentum (GeV/c)
α + Cu → p (0,180) 2.1 GeV/A
• 0° Anderson, et al.
∘ 180° Schroeder, et al.
(Preliminary)
XBL 797-2272

Fig. 1

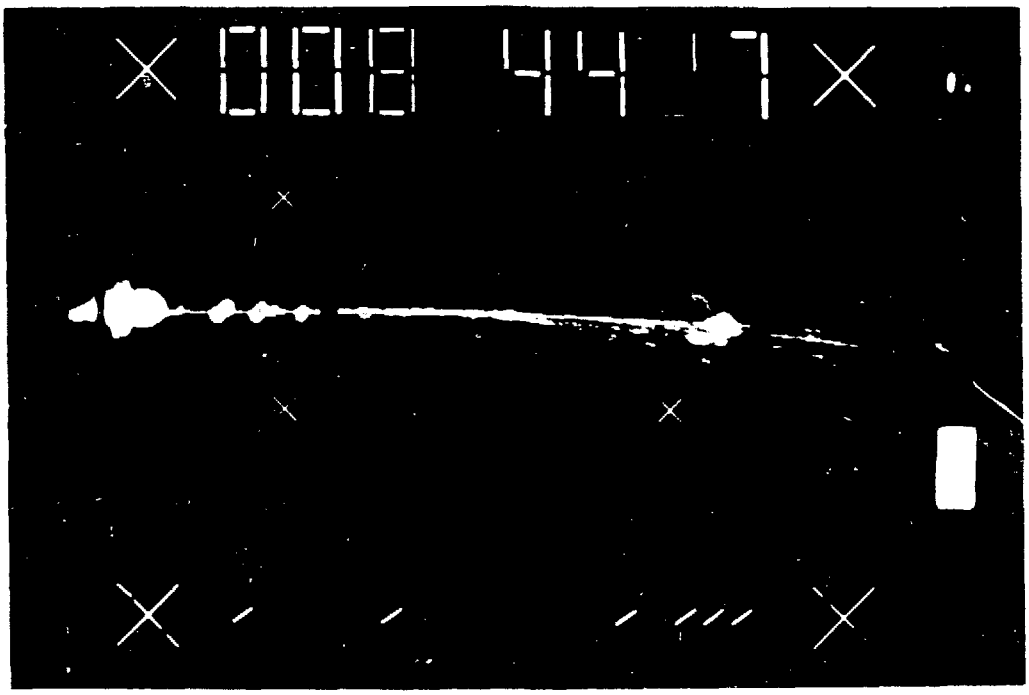

Fig. 2a

XBB 749-5727

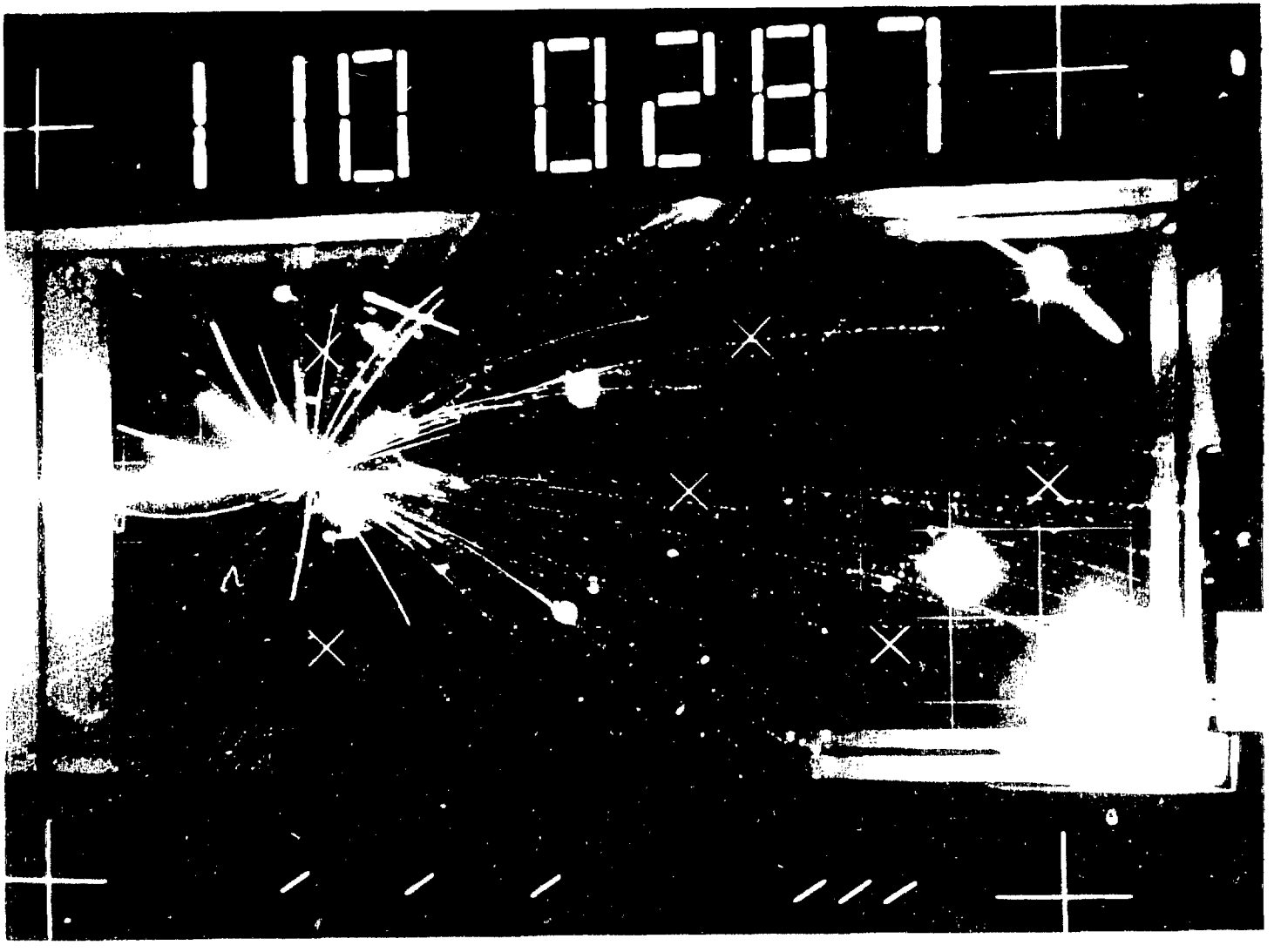

Fig. 2b

XBB 7511-8445

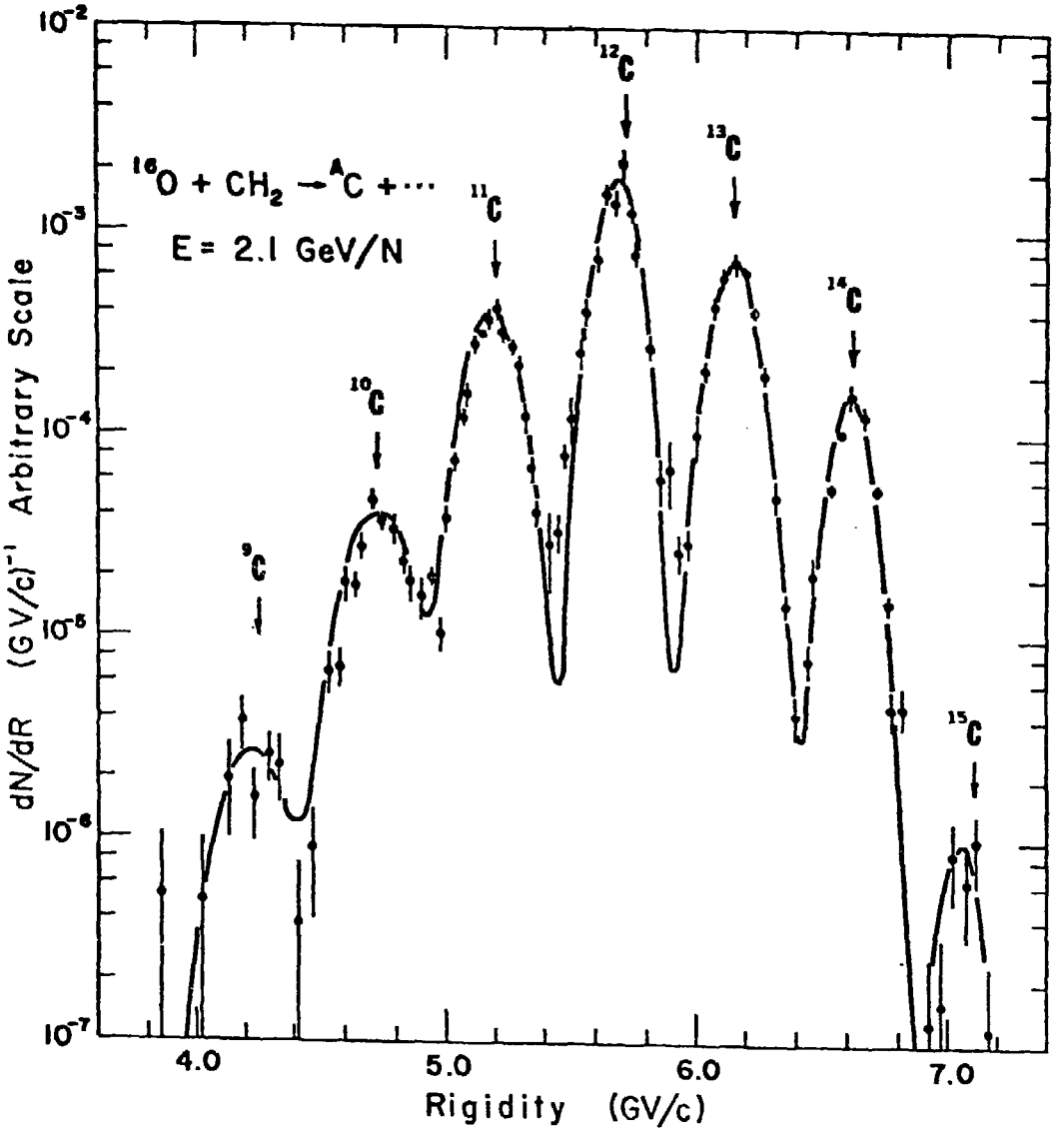

XBL 753-410

Fig. 3

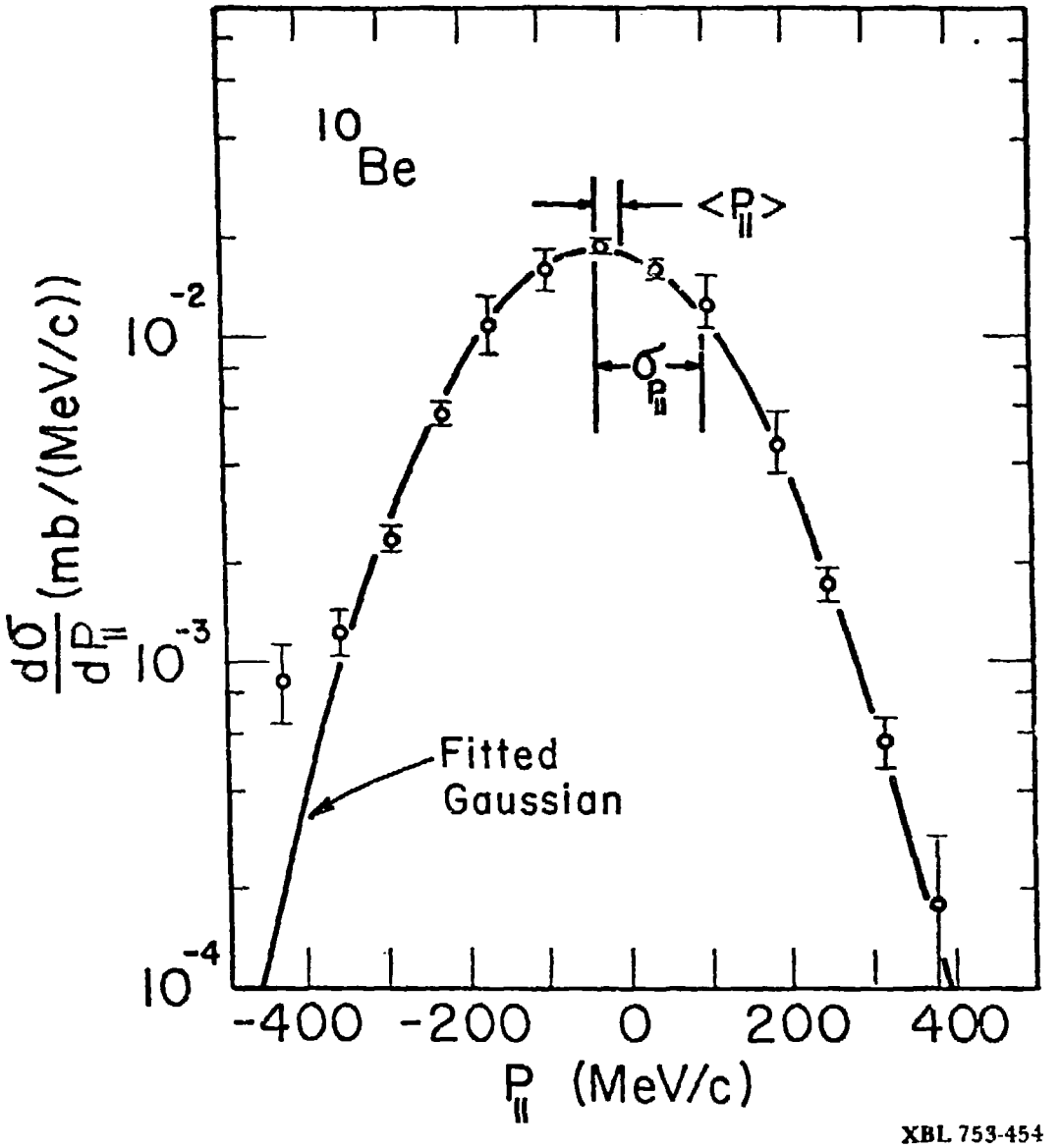

XBL 753-454

Fig. 4

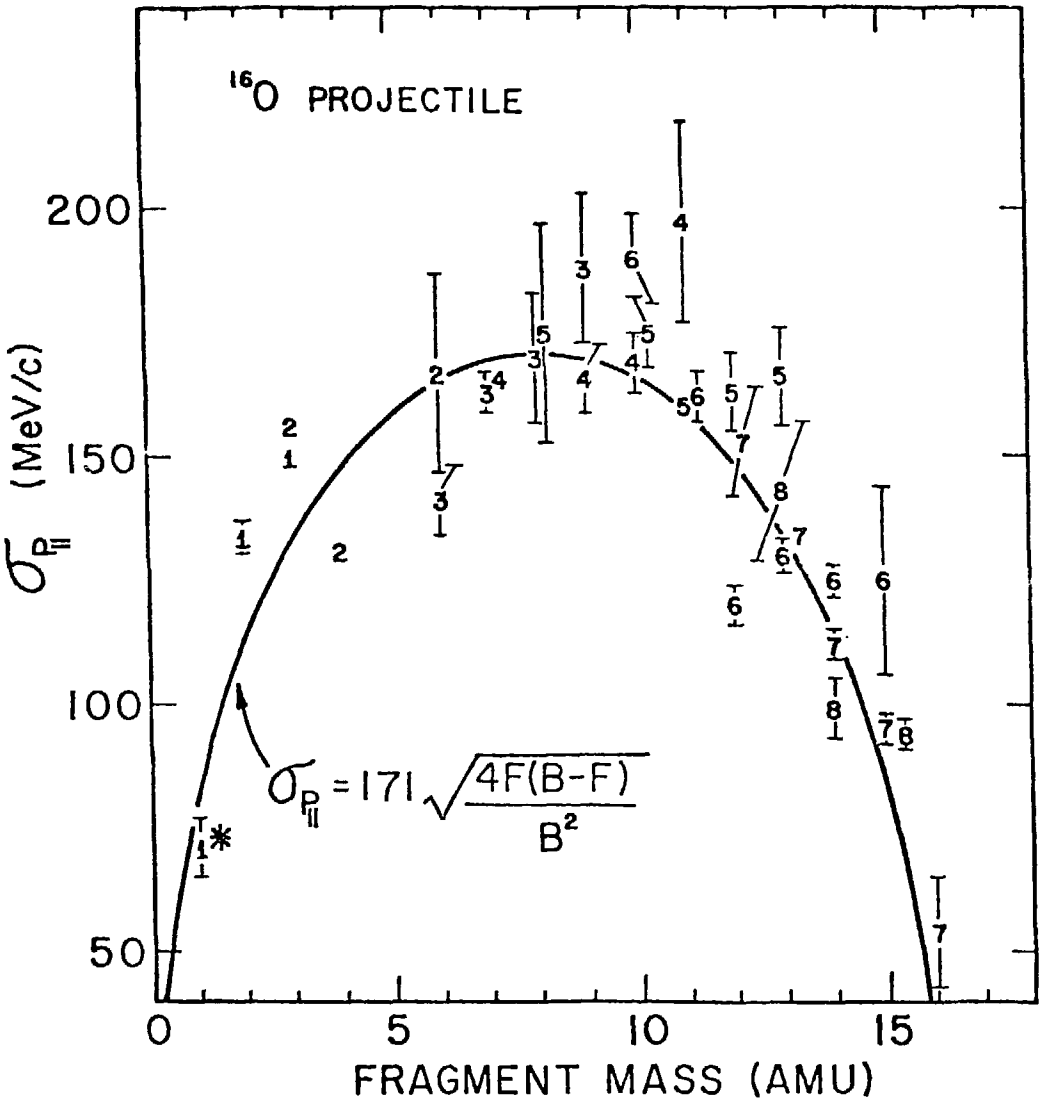

XBL 753-453

Fig. 5

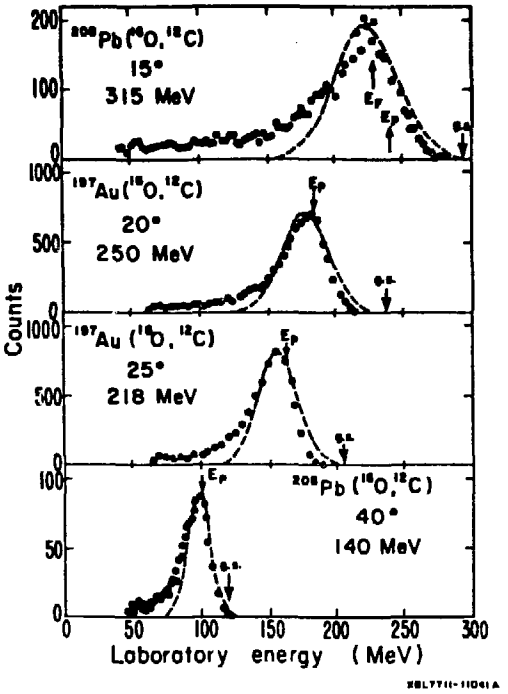
^{208}Pb(^{16}O,^{12}C)
15°
315 MeV
^{197}Au(^{16}O,^{12}C)
20°
250 MeV
^{197}Au(^{16}O,^{12}C)
25°
218 MeV
^{208}Pb(^{16}O,^{12}C)
40°
140 MeV
Counts
Laboratory energy (MeV)

Fig. 6

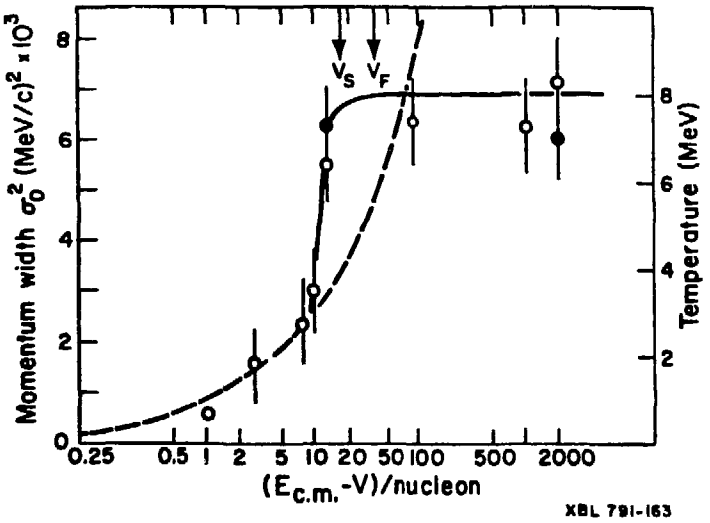
Momentum width σ_0^2 (MeV/c)^2 x10^3
Temperature (MeV)
V_S
V_F
($E_{c.m.}$-V)/nucleon
XBL 791-163

Fig. 7

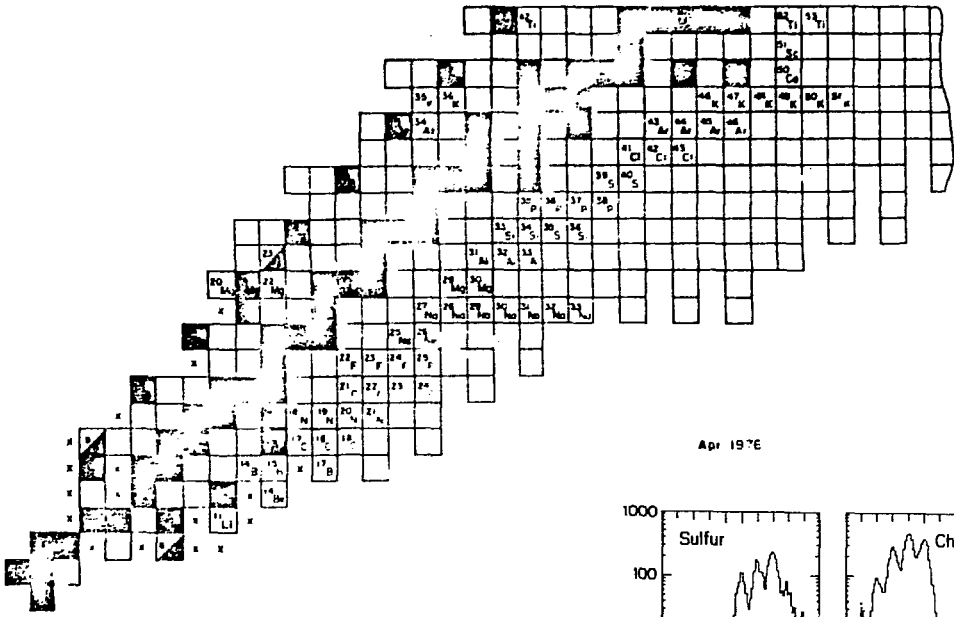

Fig. 8

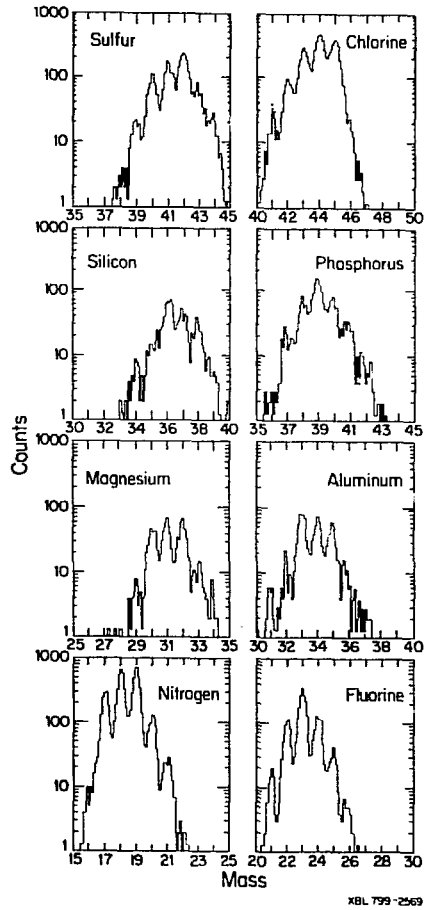
Sulfur
Chlorine
Silicon
Phosphorus
Magnesium
Aluminum
Nitrogen
Fluorine
Counts
Mass
1000
100
10
1
35 37 39 41 43 45
40 42 44 46 48 50
30 32 34 36 38 40
25 27 29 31 33 35
15 17 19 21 23 25
20 22 24 26 28 30
XBL 799-2569

Fig. 9

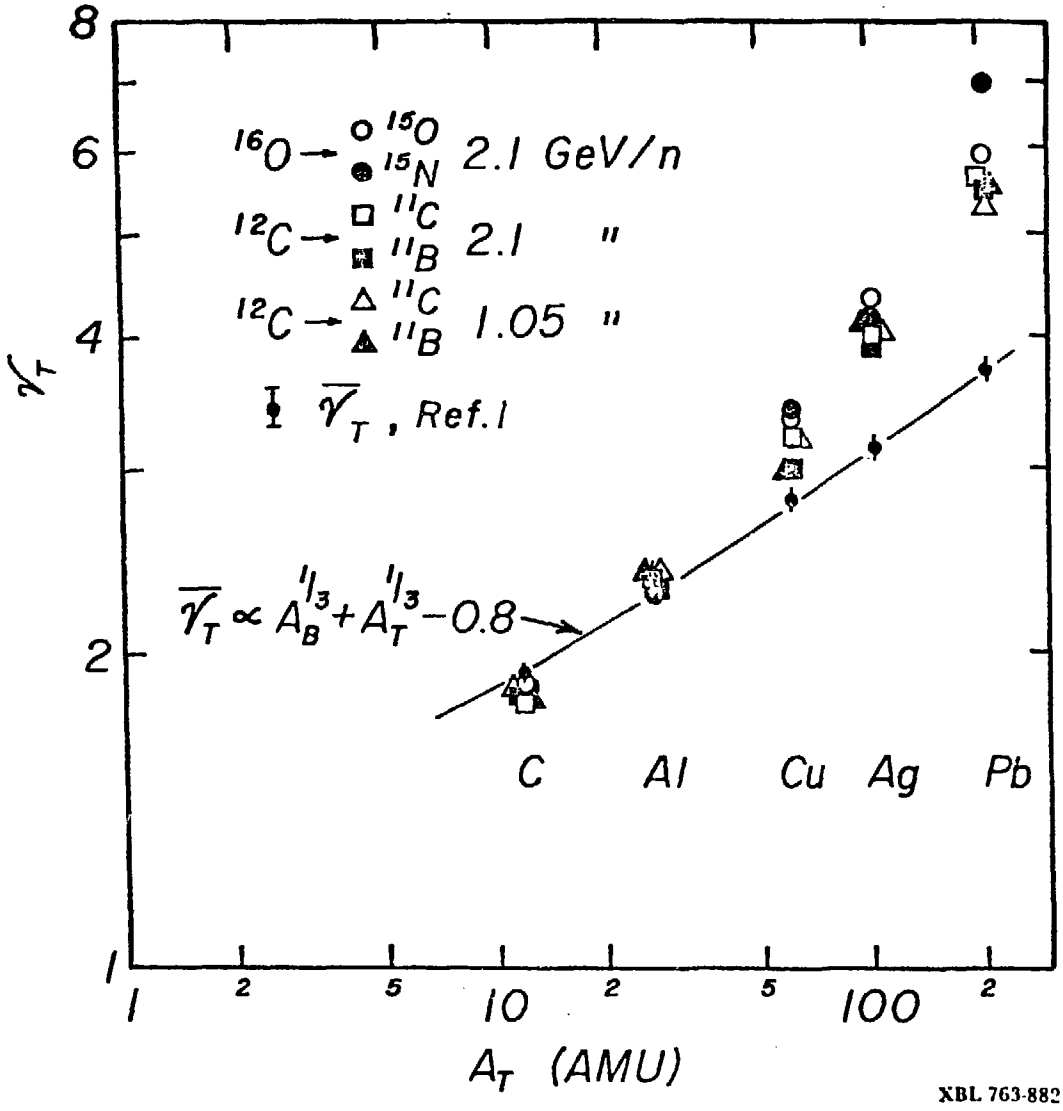

XBL 763-882

Fig. 10

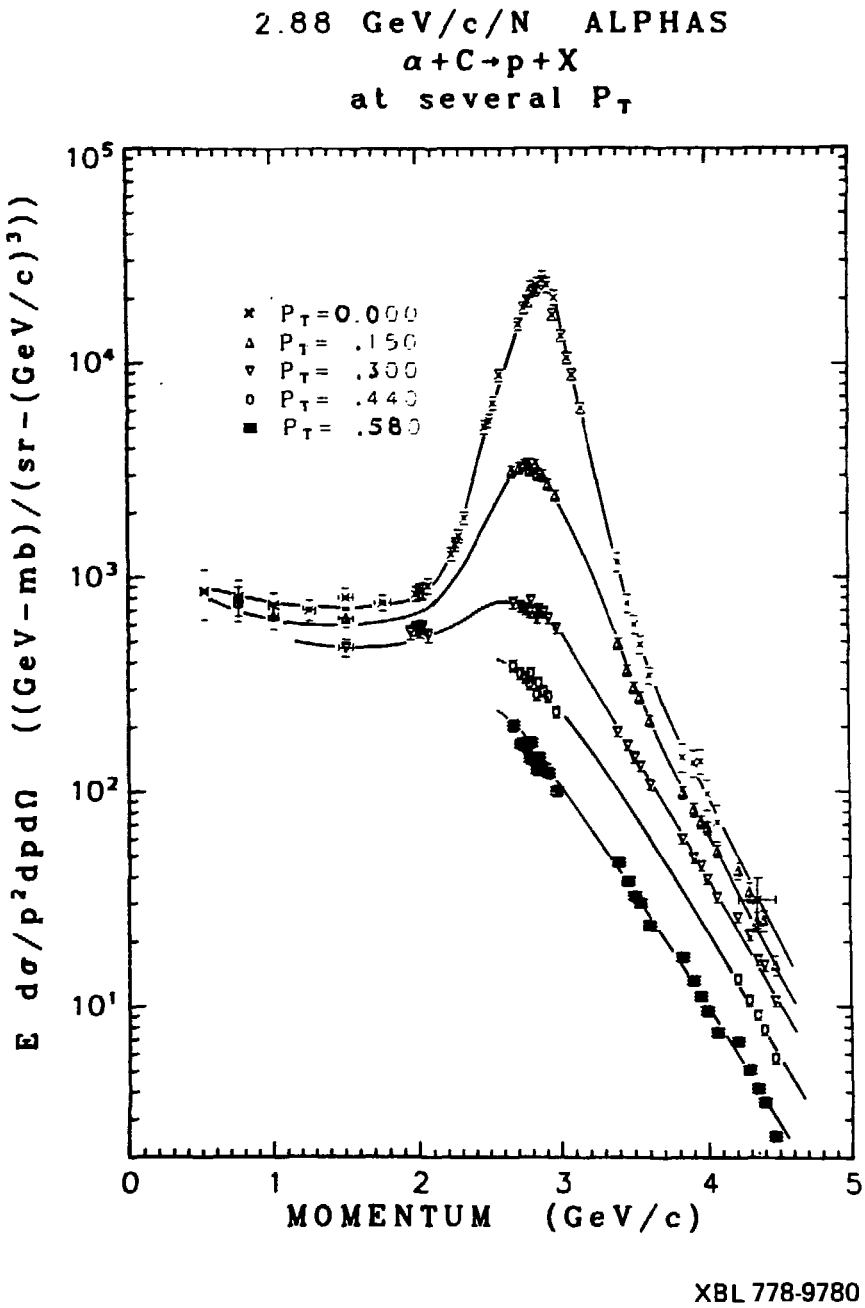
2.88 GeV/c/N ALPHAS
α+C→p+X
at several P_T
P_T=0.000
P_T= .150
P_T= .300
P_T= .440
P_T= .580
E dσ/p²dpdΩ ((GeV-mb)/(sr-(GeV/c)³))
MOMENTUM (GeV/c)
XBL 778-9780

Fig. 11

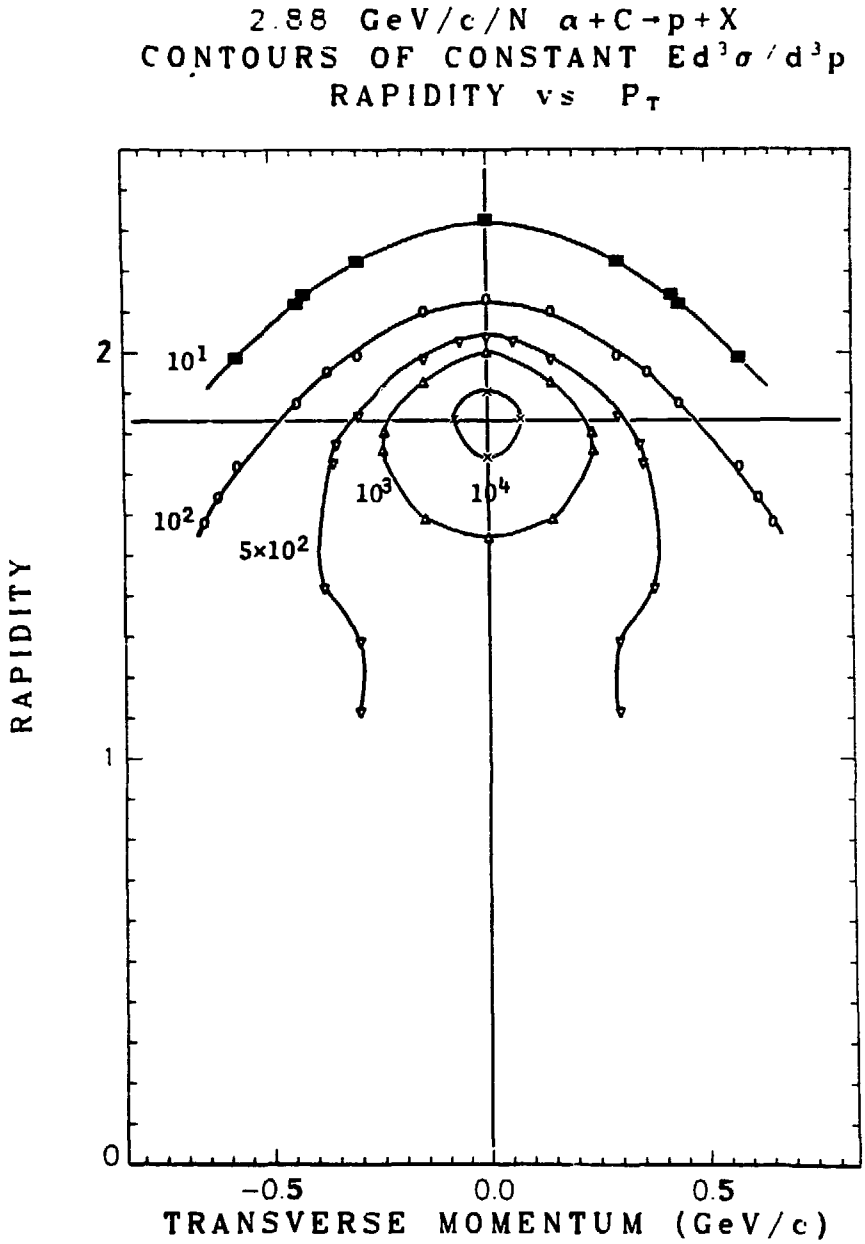

XBL 779-2457

Fig. 12

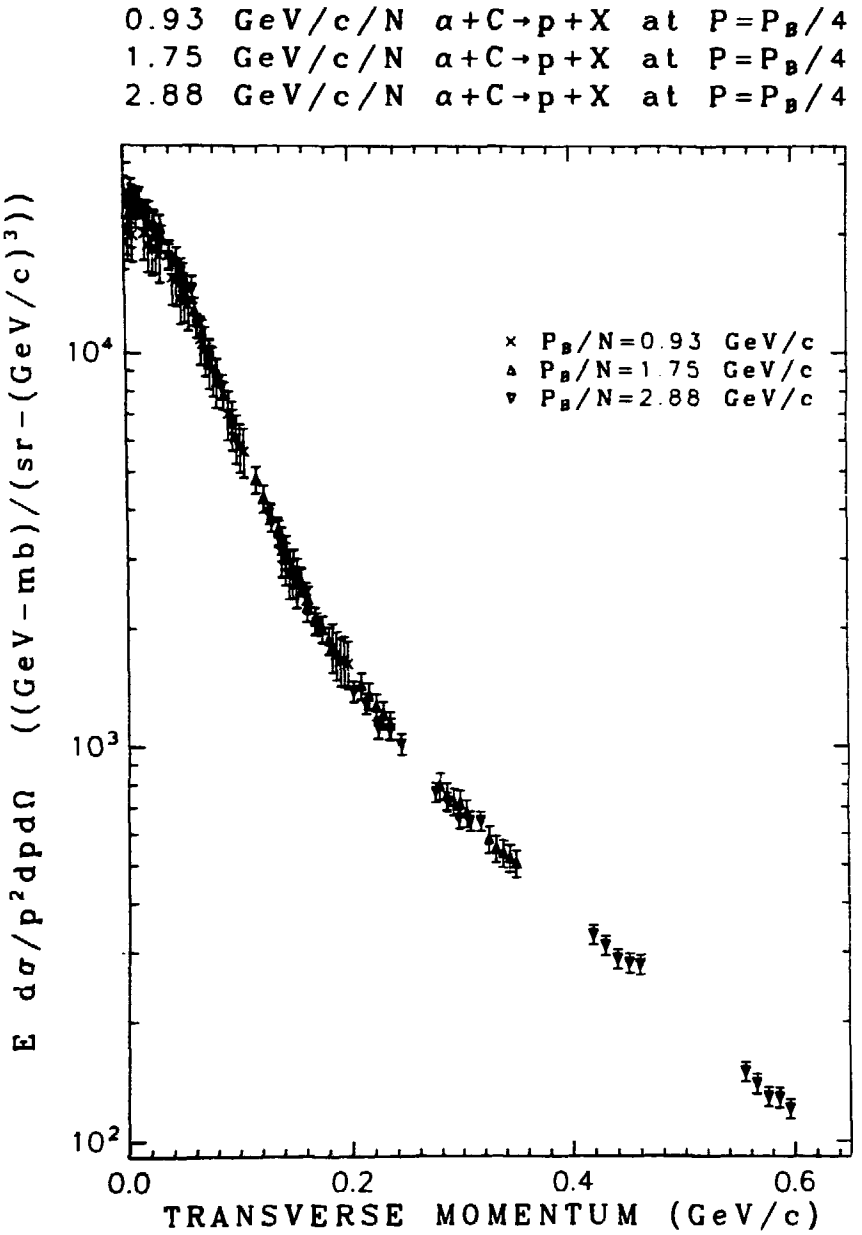

XBL 778-2602

Fig. 13

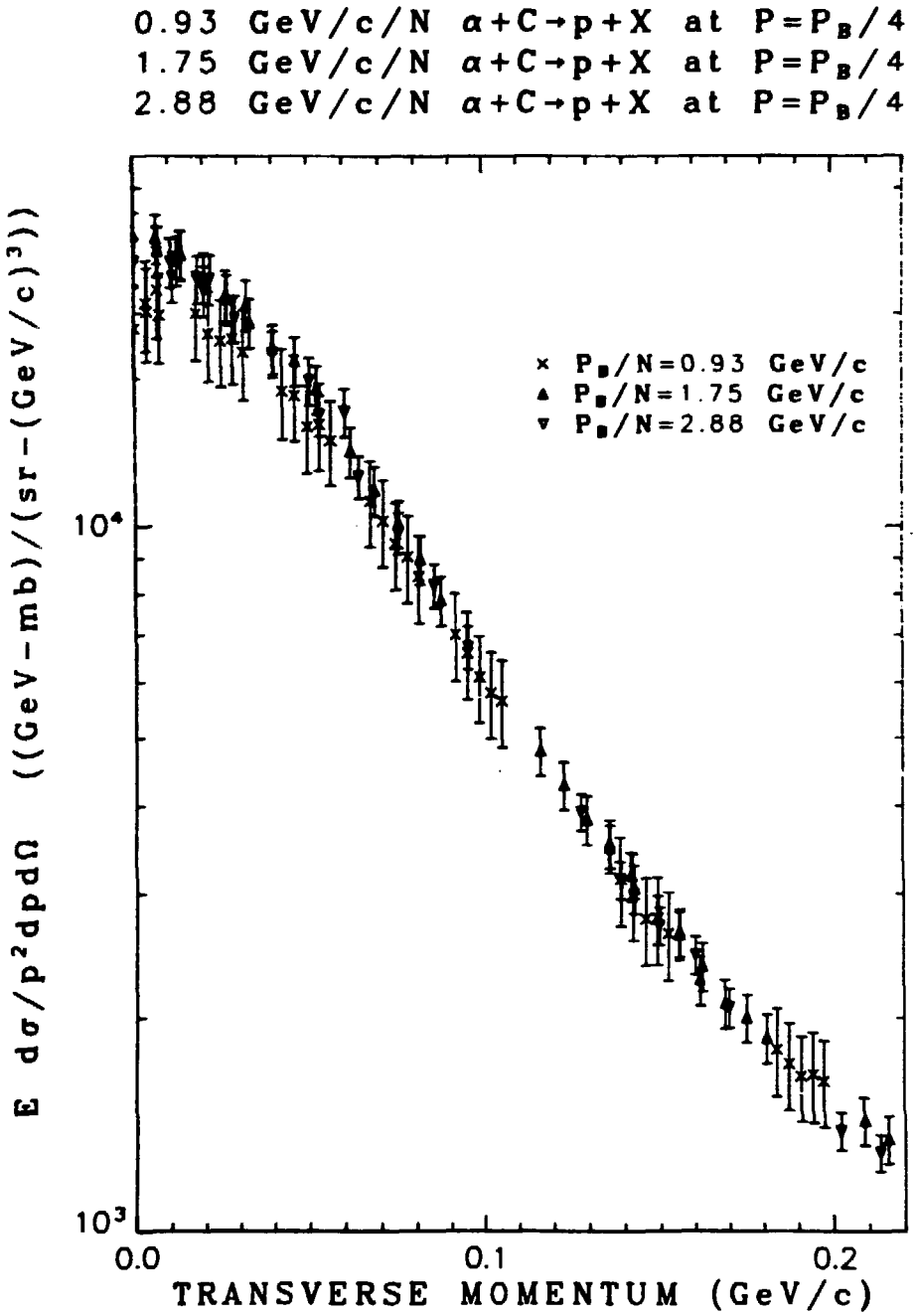

XBL 778-2600

Fig. 14

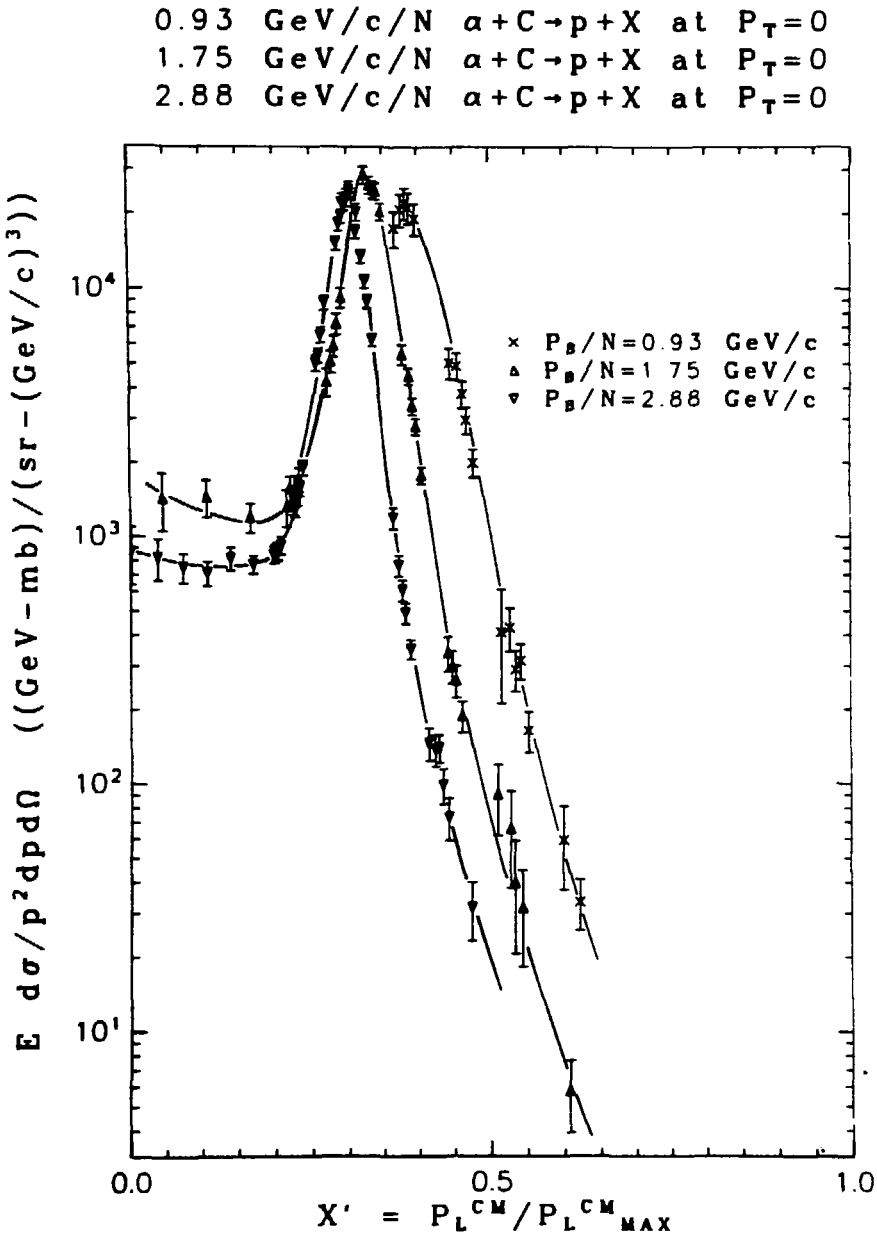

XBL 778-2604

Fig. 15

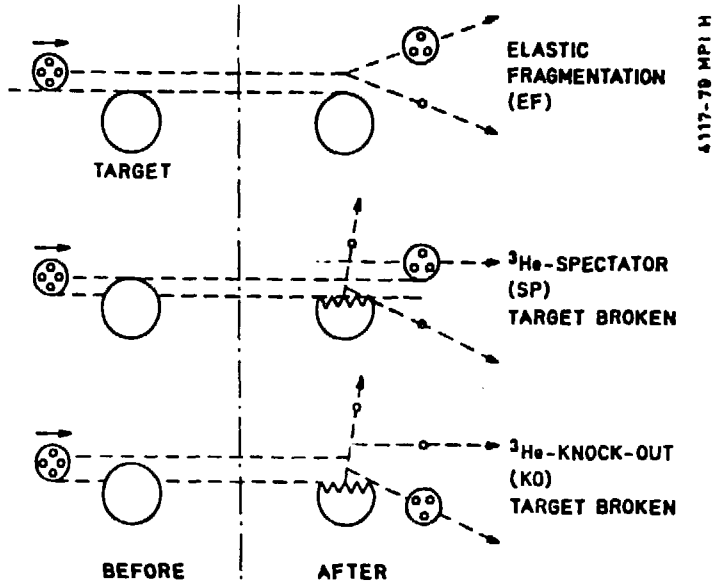
ELASTIC
FRAGMENTATION
(EF)
TARGET
^{3}He-SPECTATOR
(SP)
TARGET BROKEN
^{3}He-KNOCK-OUT
(KO)
TARGET BROKEN
BEFORE
AFTER
4117-79 MPI H

Fig. 16

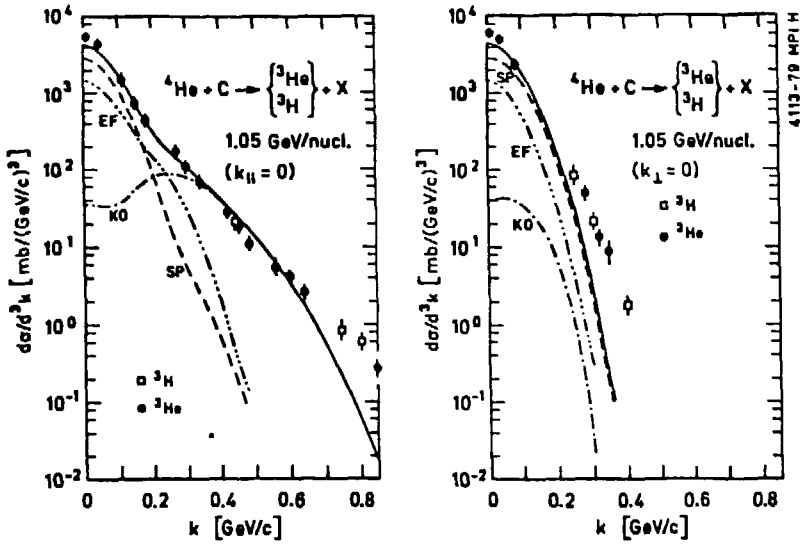
^{4}He + C → {^{3}He, ^{3}H} + X
1.05 GeV/nucl.
($k_{\parallel}$ = 0)
($k_{\perp}$ = 0)
EF
KO
SP
□ ^{3}H
● ^{3}He
dσ/d^{3}k [mb/(GeV/c)^3]
k [GeV/c]
4113-79 MPI H

Fig. 17

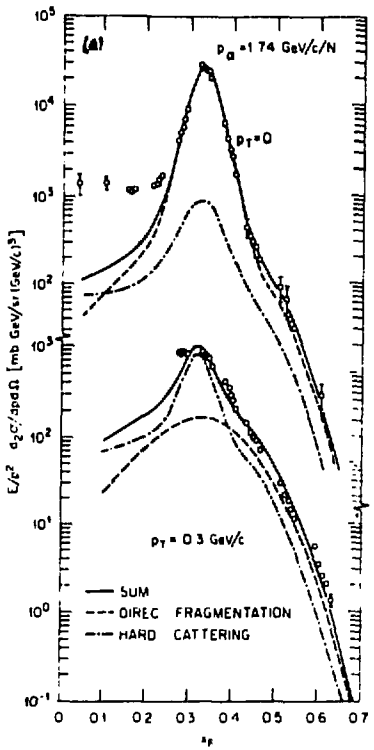
(a)
p_a = 1.74 GeV/c/N
p_T = 0
p_T = 0.3 GeV/c
SUM
DIREC FRAGMENTATION
HARD CATTERING

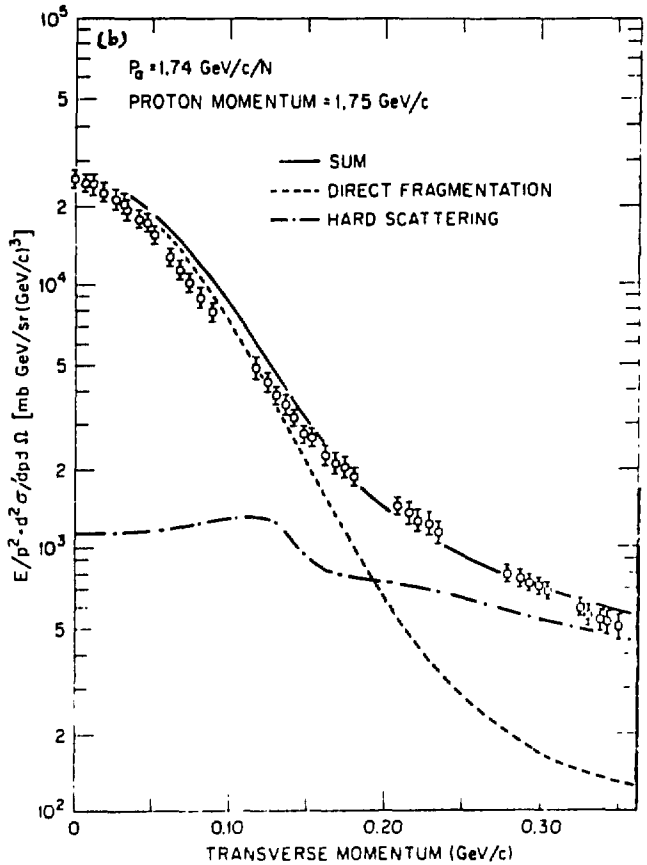
(b)
P_a = 1.74 GeV/c/N
PROTON MOMENTUM = 1.75 GeV/c
SUM
DIRECT FRAGMENTATION
HARD SCATTERING
$E/p^2 \cdot d^2\sigma/dp\,d\Omega$ [mb GeV/sr (GeV/c)^3]
TRANSVERSE MOMENTUM (GeV/c)

Fig. 19

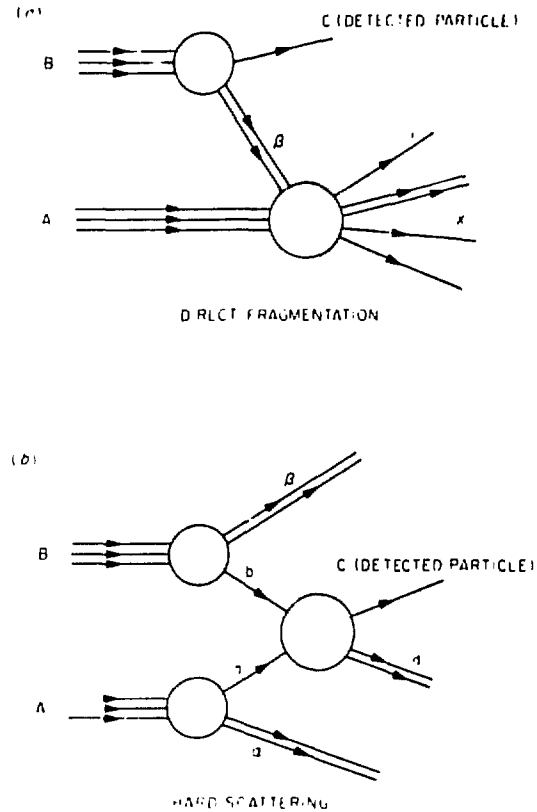
C (DETECTED PARTICLE)
B
A
DIRECT FRAGMENTATION
C (DETECTED PARTICLE)
B
A
HARD SCATTERING

Fig. 18

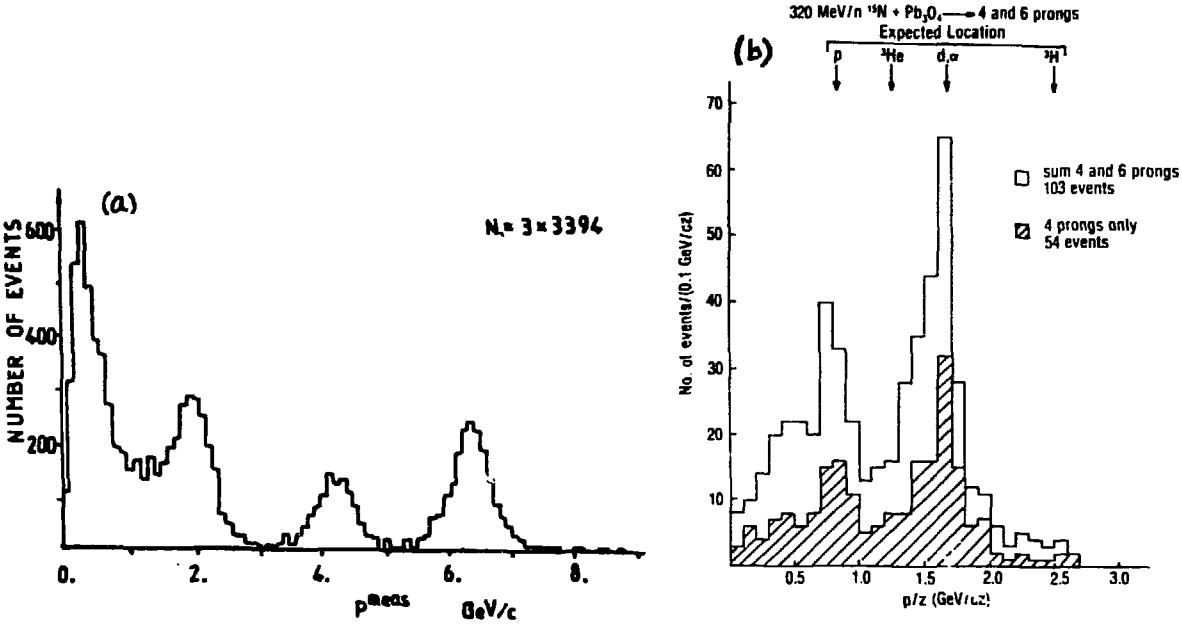
(a)
NUMBER OF EVENTS
600
400
200
N.= 3×3394
0.
2.
4.
6.
8.
p^meas GeV/c
320 MeV/n ¹⁵N + Pb₃O₄ → 4 and 6 prongs
Expected Location
(b)
p
³He
d,α
³H
70
60
50
40
30
20
10
No. of events/(0.1 GeV/cz)
sum 4 and 6 prongs
103 events
4 prongs only
54 events
0.5
1.0
1.5
2.0
2.5
3.0
p/z (GeV/cz)

Fig. 20

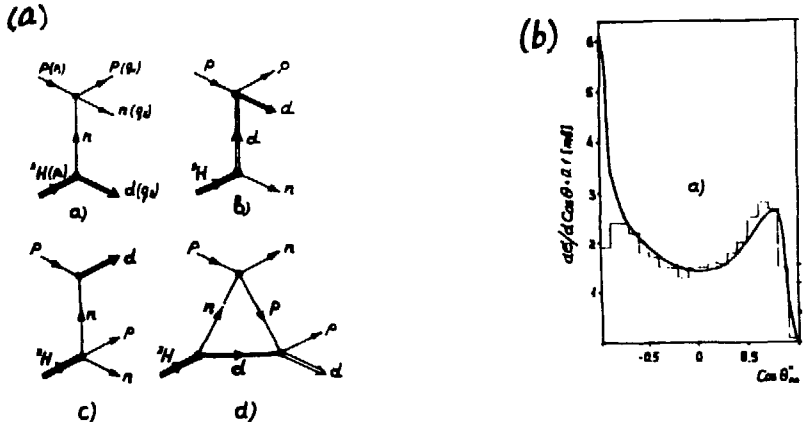
(a)
P(n)
P(q_p)
n(q_n)
n
²H(A)
d(q_d)
a)
p
p
d
d
²H
n
b)
p
d
n
²H
p
n
c)
p
n
n
p
²H
d
p
d
d)
(b)
a)
-0.5
0
0.5

Fig. 21

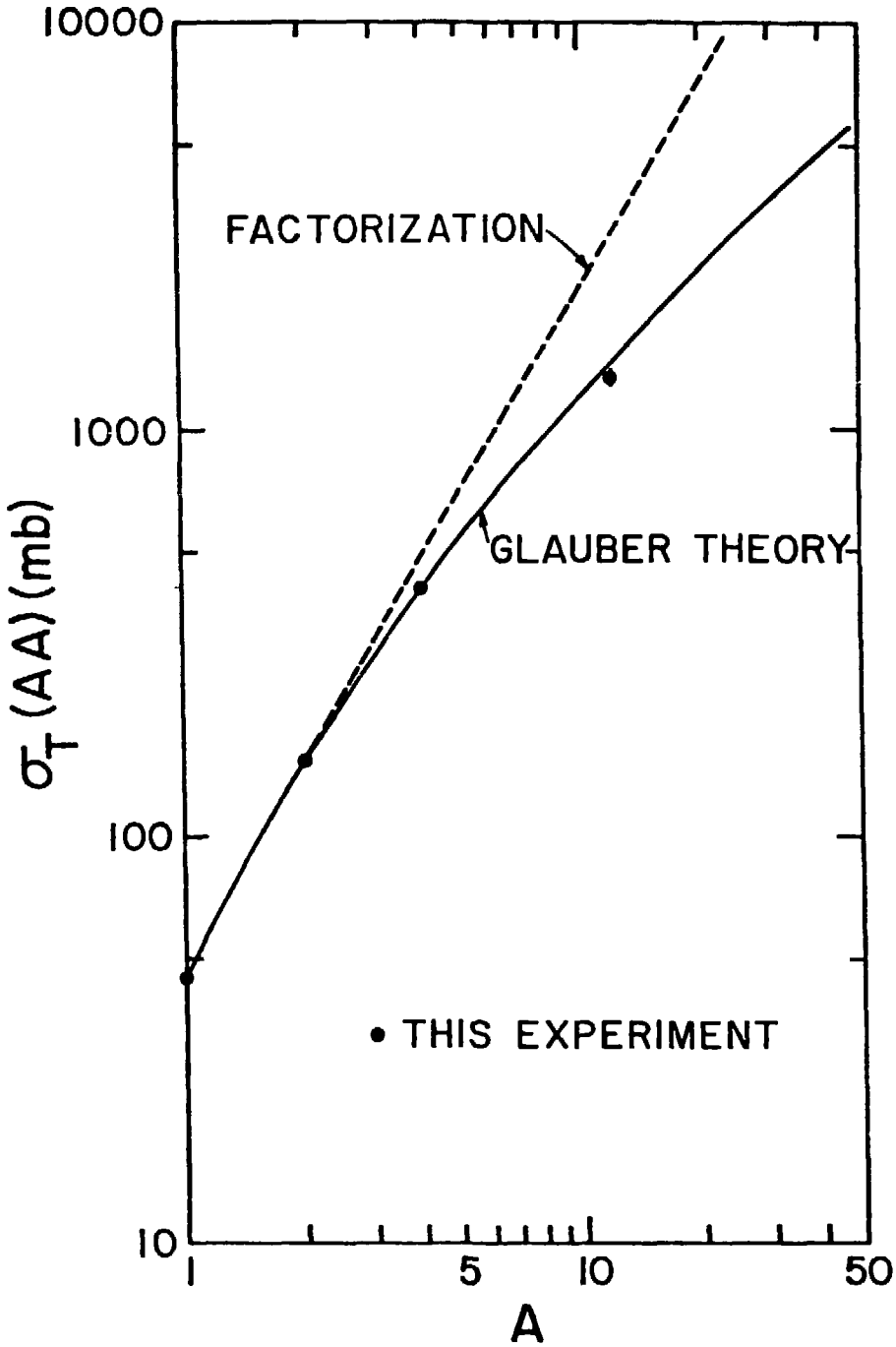
10000
1000
100
10
σ_T (AA) (mb)
FACTORIZATION
GLAUBER THEORY
• THIS EXPERIMENT
1
5
10
50
A

Fig. 22

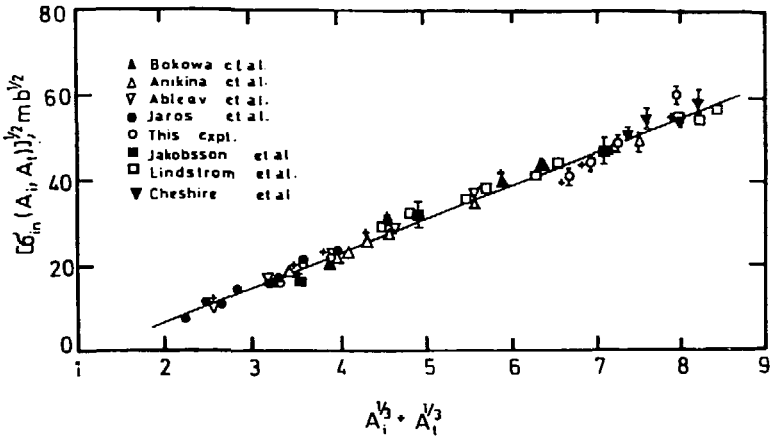
80
60
40
20
0
1
2
3
4
5
6
7
8
9
▲ Bokowa et al.
△ Anikina et al.
▽ Ableev et al.
● Jaros et al.
○ This expt.
■ Jakobsson et al
□ Lindstrom et al.
▼ Cheshire et al
$[\sigma_{in}(A_i, A_t)]^{1/2}$, mb$^{1/2}$
$A_i^{1/3} + A_t^{1/3}$

Fig. 23

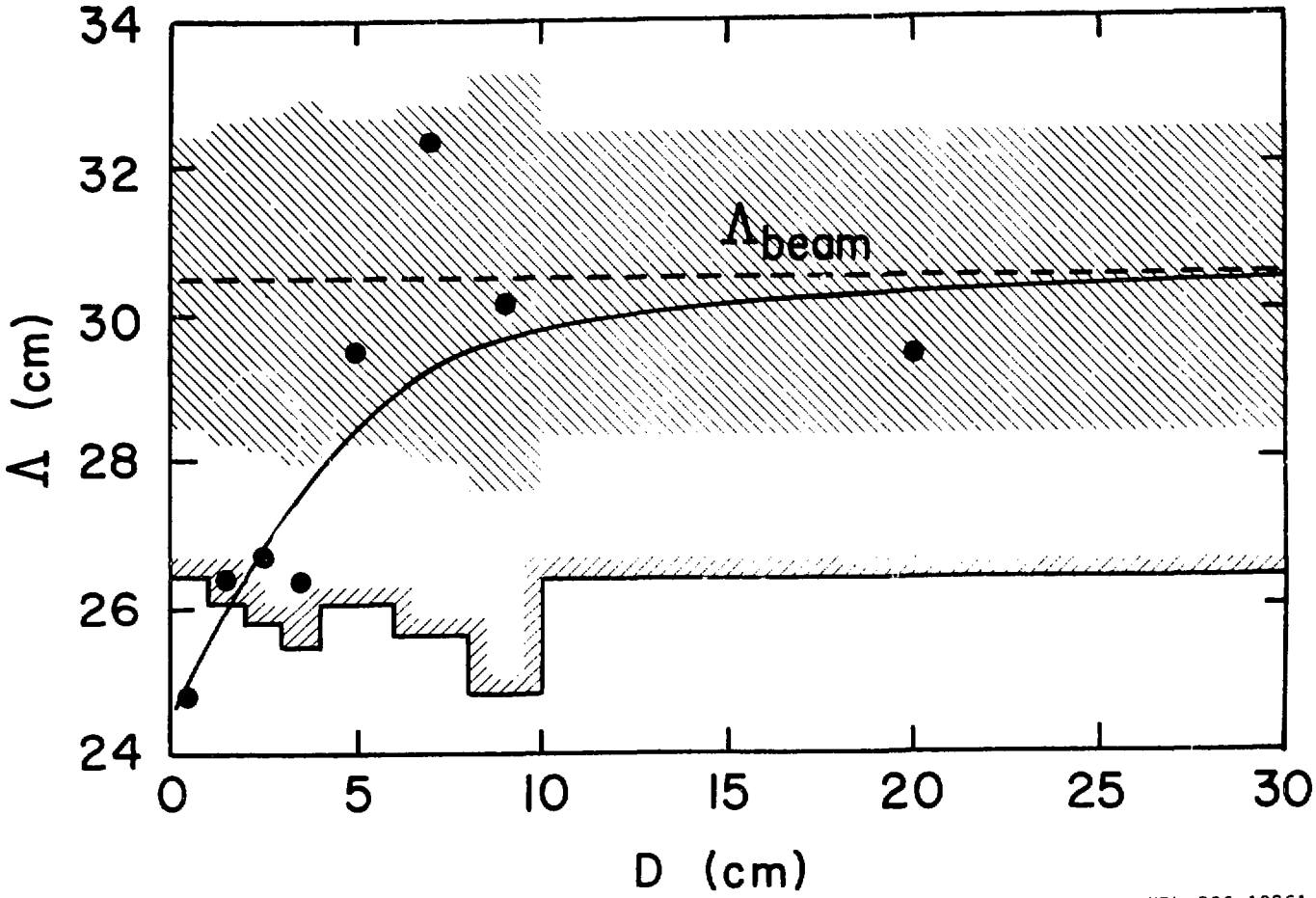

XBL 806-10261

Fig. 24

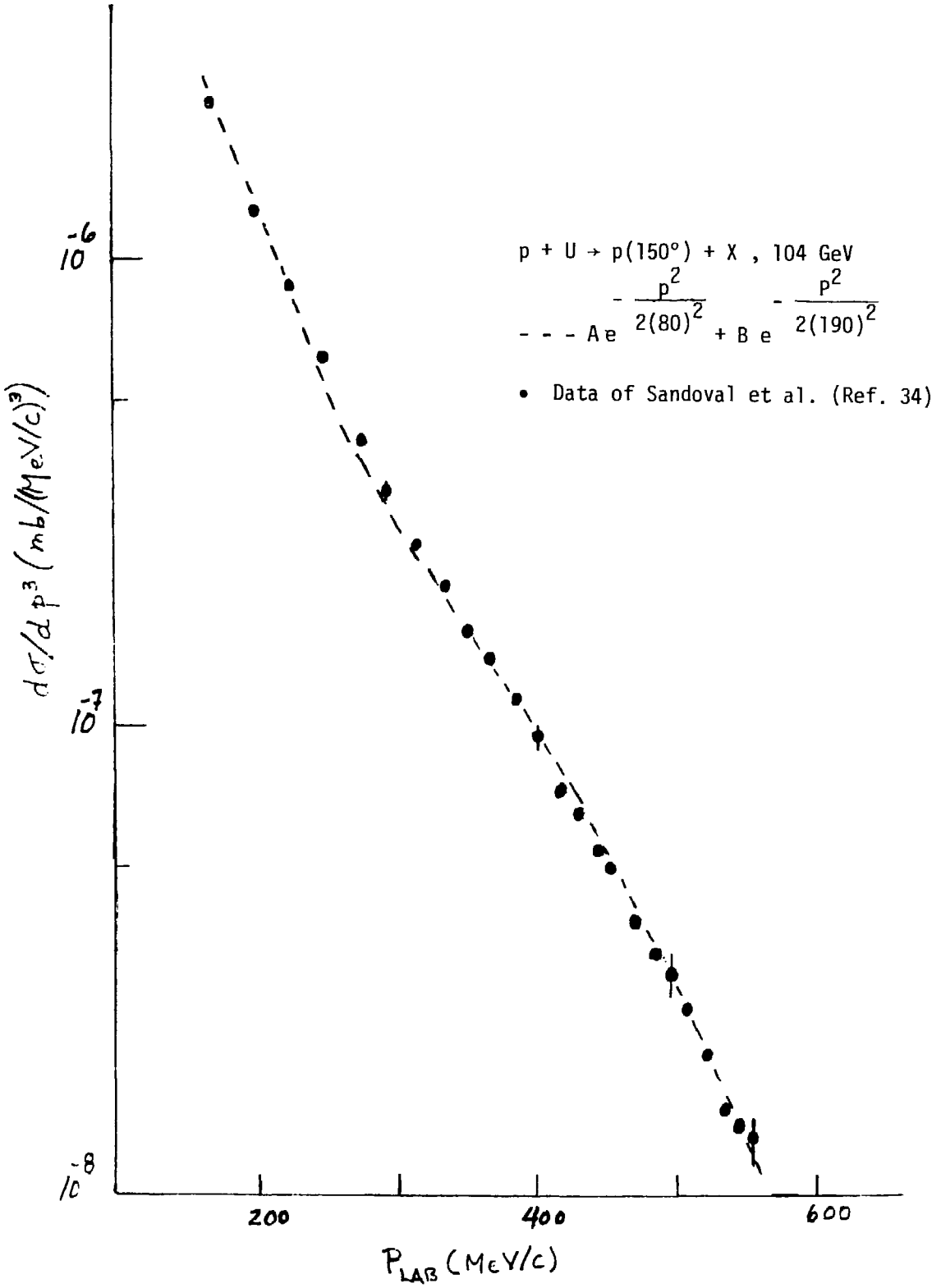
p + U → p(150°) + X , 104 GeV
- - - $Ae^{-\frac{p^2}{2(80)^2}} + Be^{-\frac{p^2}{2(190)^2}}$
• Data of Sandoval et al. (Ref. 34)
10^{-6}
10^{-7}
10^{-8}
$d\sigma/dp^3$ (mb/(MeV/c)^3)
200
400
600
P_{LAB} (MeV/c)

Fig. 25

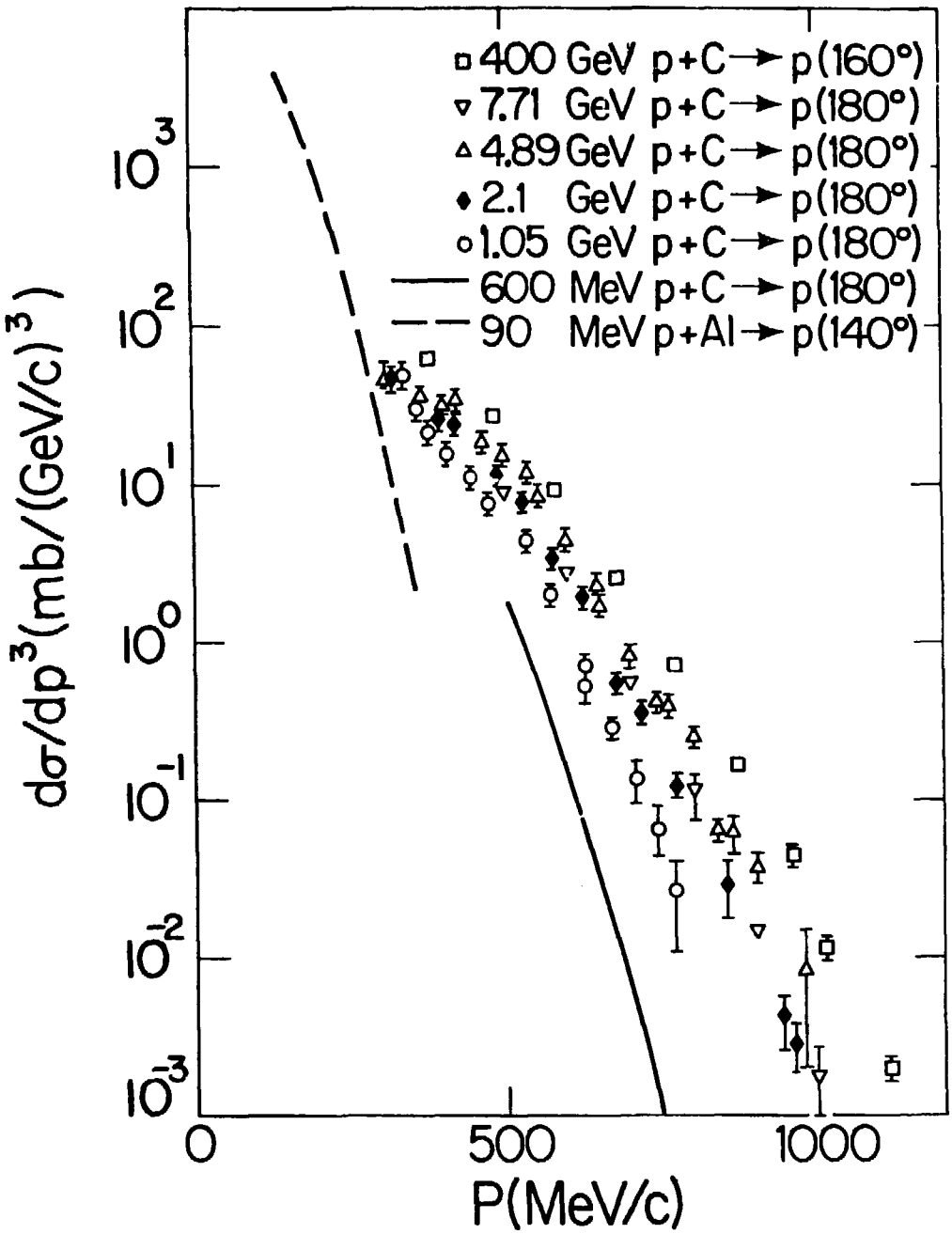

XBL 7912-13375

Fig. 26

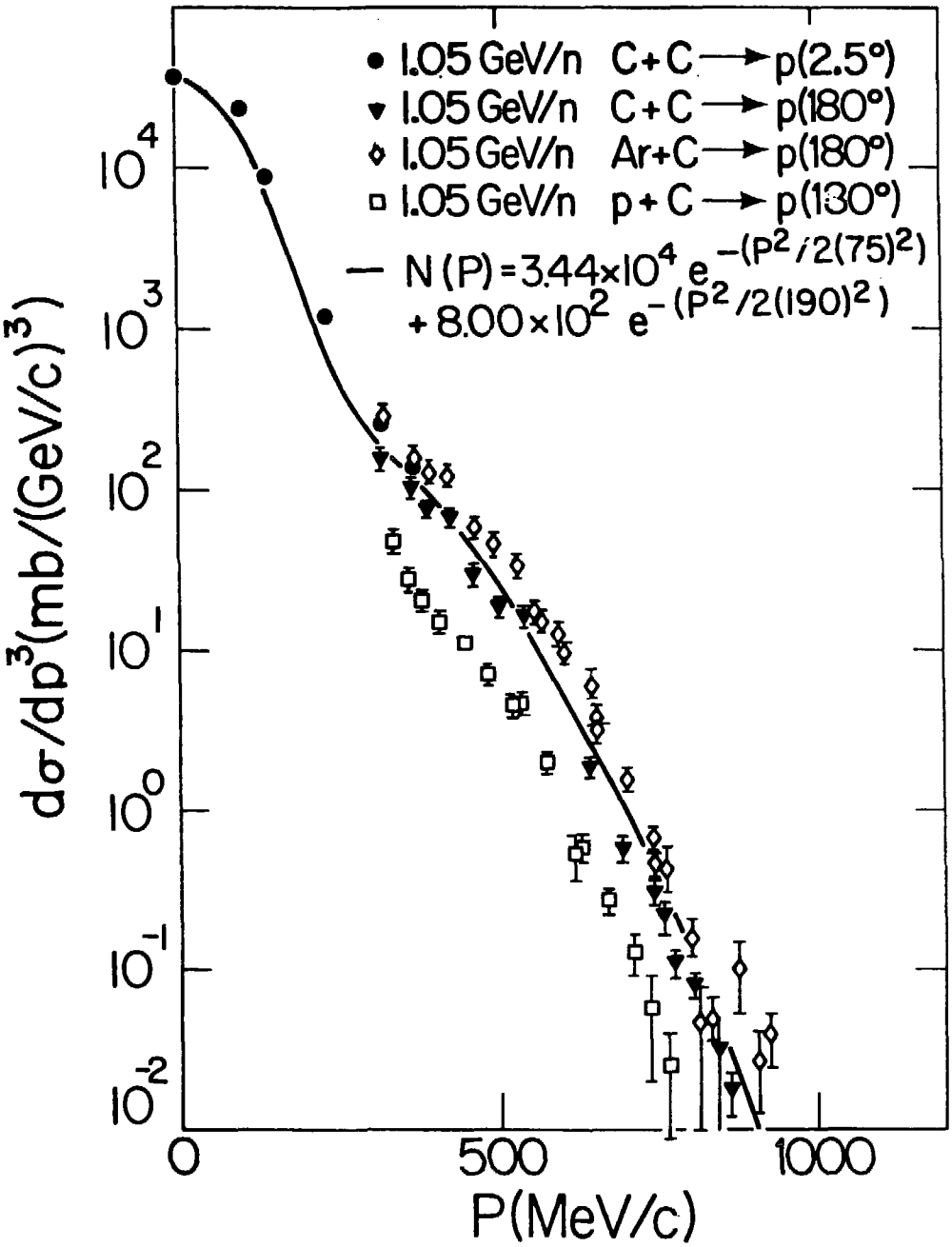

XBL 7912-13374

Fig. 27

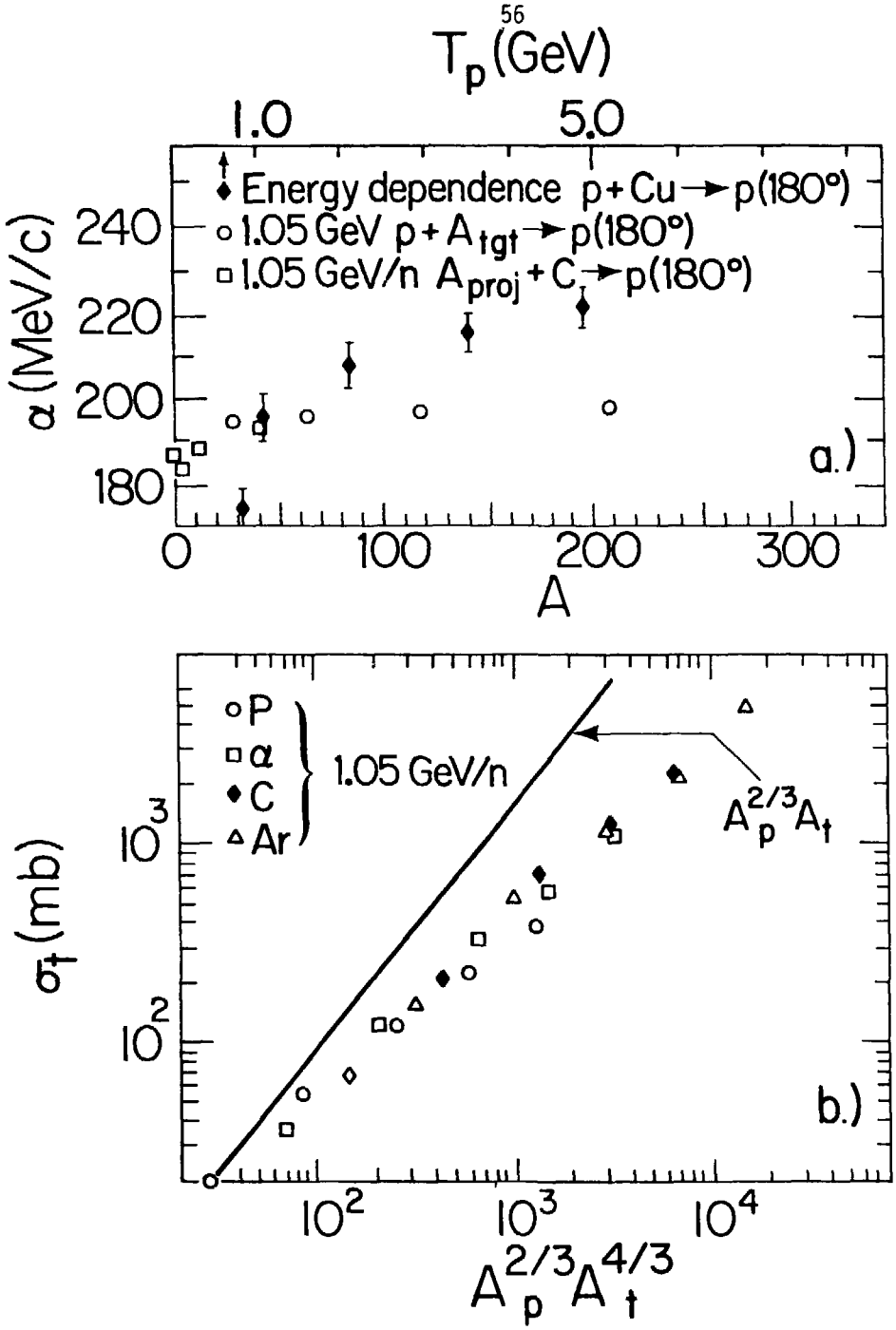

XBL 7912-13376

Fig. 28

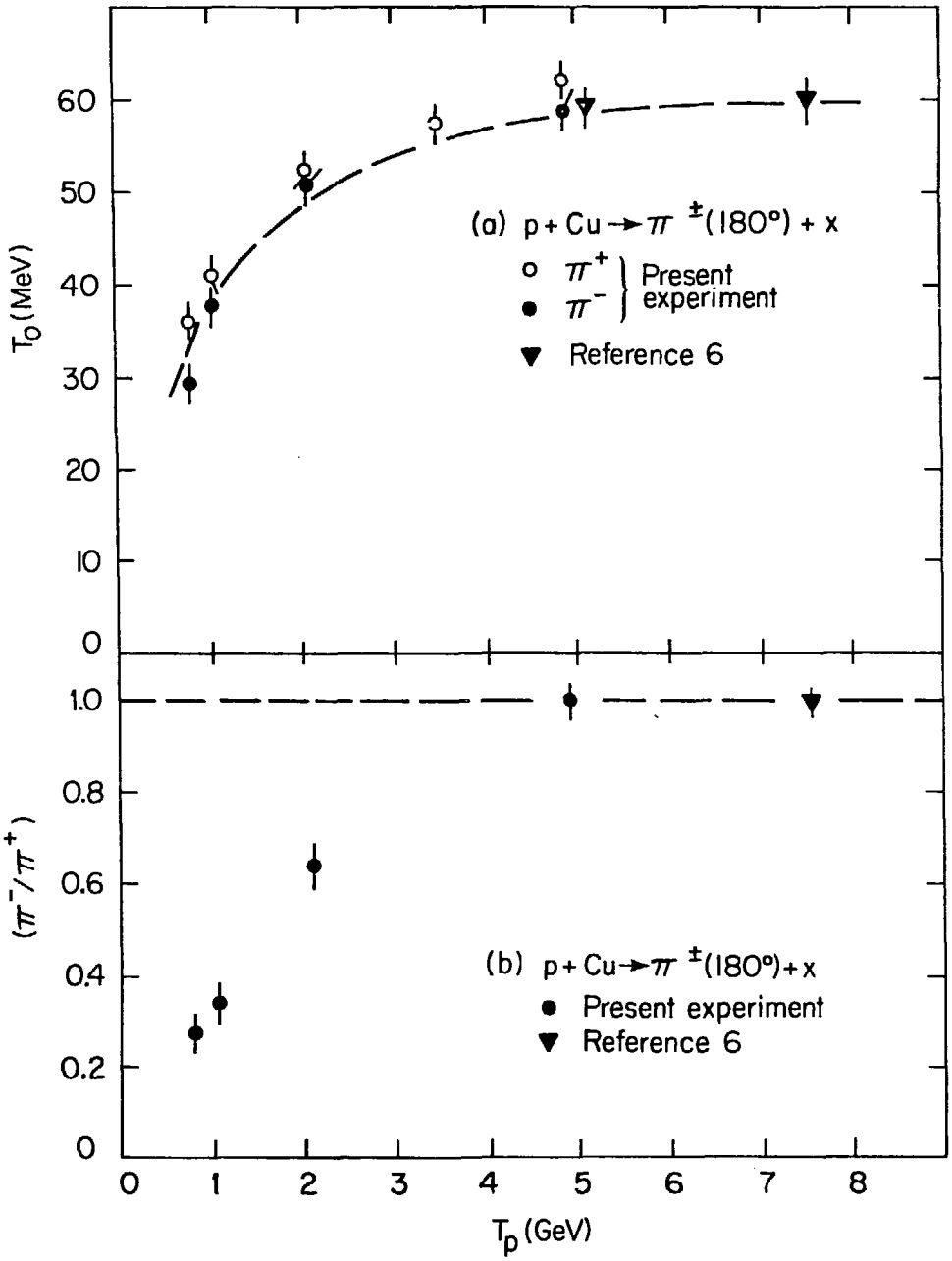

XBL 798 - 2506

Fig. 29

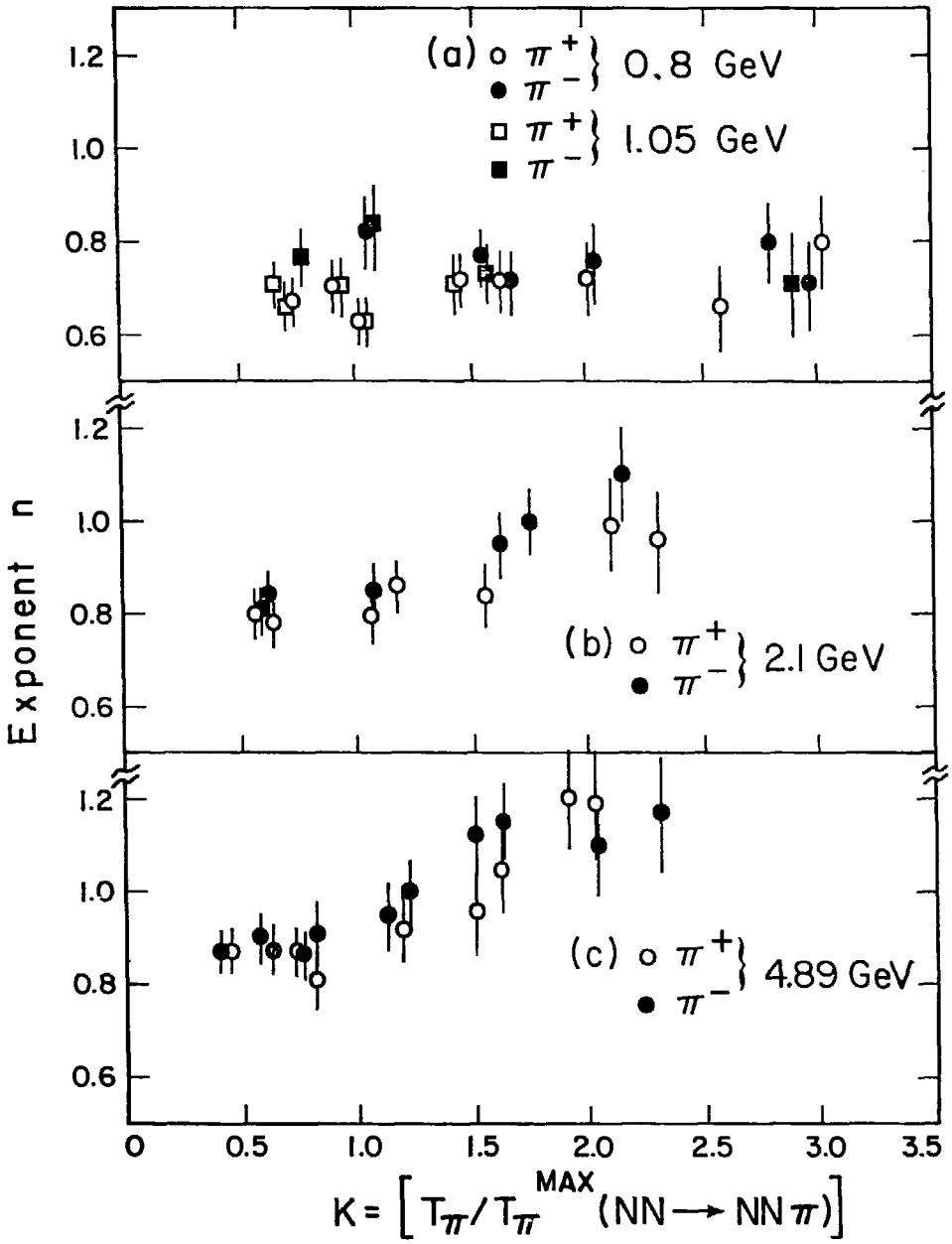

XBL 799-2812

Fig. 30

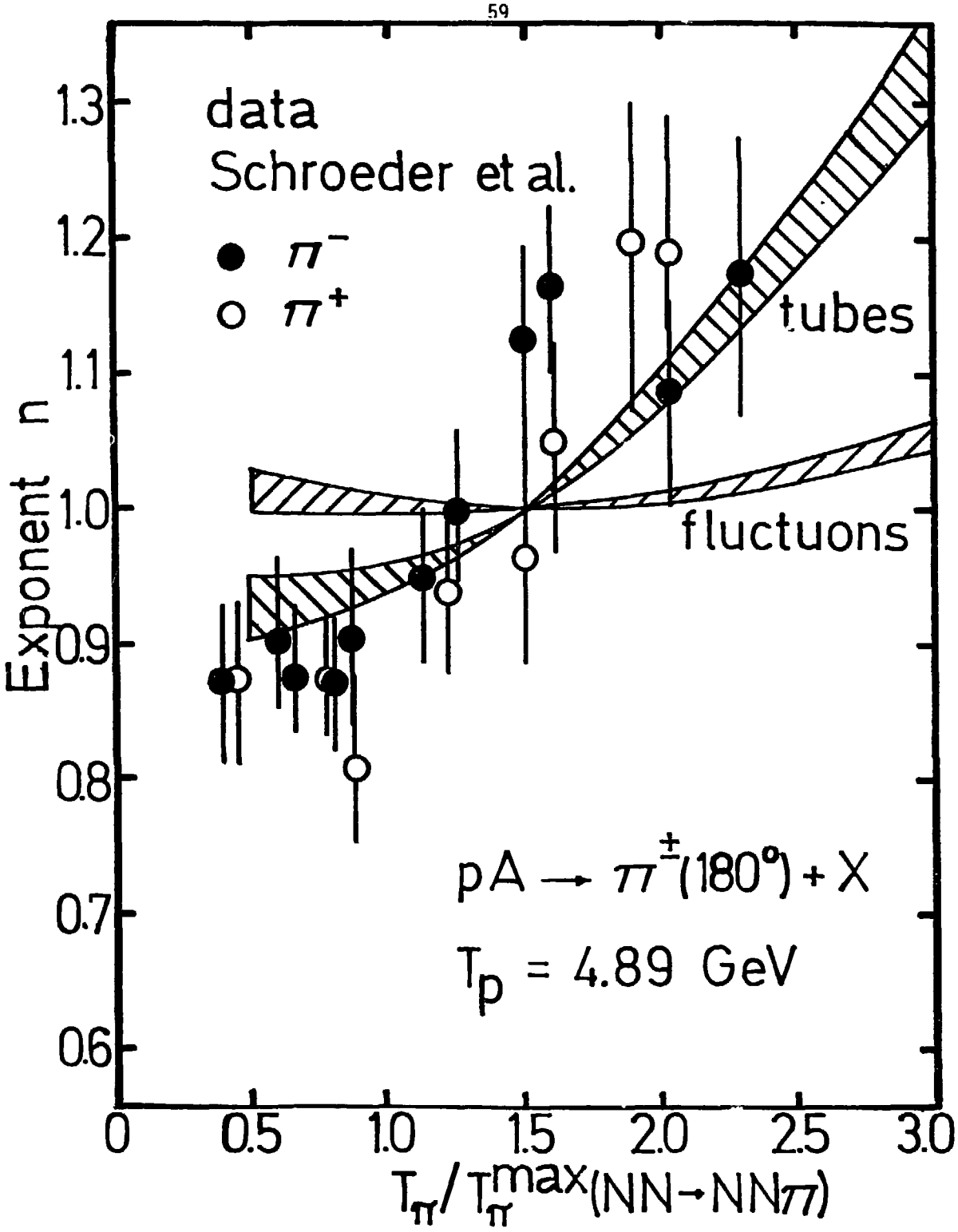
data
Schroeder et al.
π⁻
π⁺
tubes
fluctuons
pA → π±(180°) + X
Tp = 4.89 GeV
Exponent n
1.3
1.2
1.1
1.0
0.9
0.8
0.7
0.6
0
0.5
1.0
1.5
2.0
2.5
3.0
Tπ/Tπmax(NN→NNπ)

Fig. 31

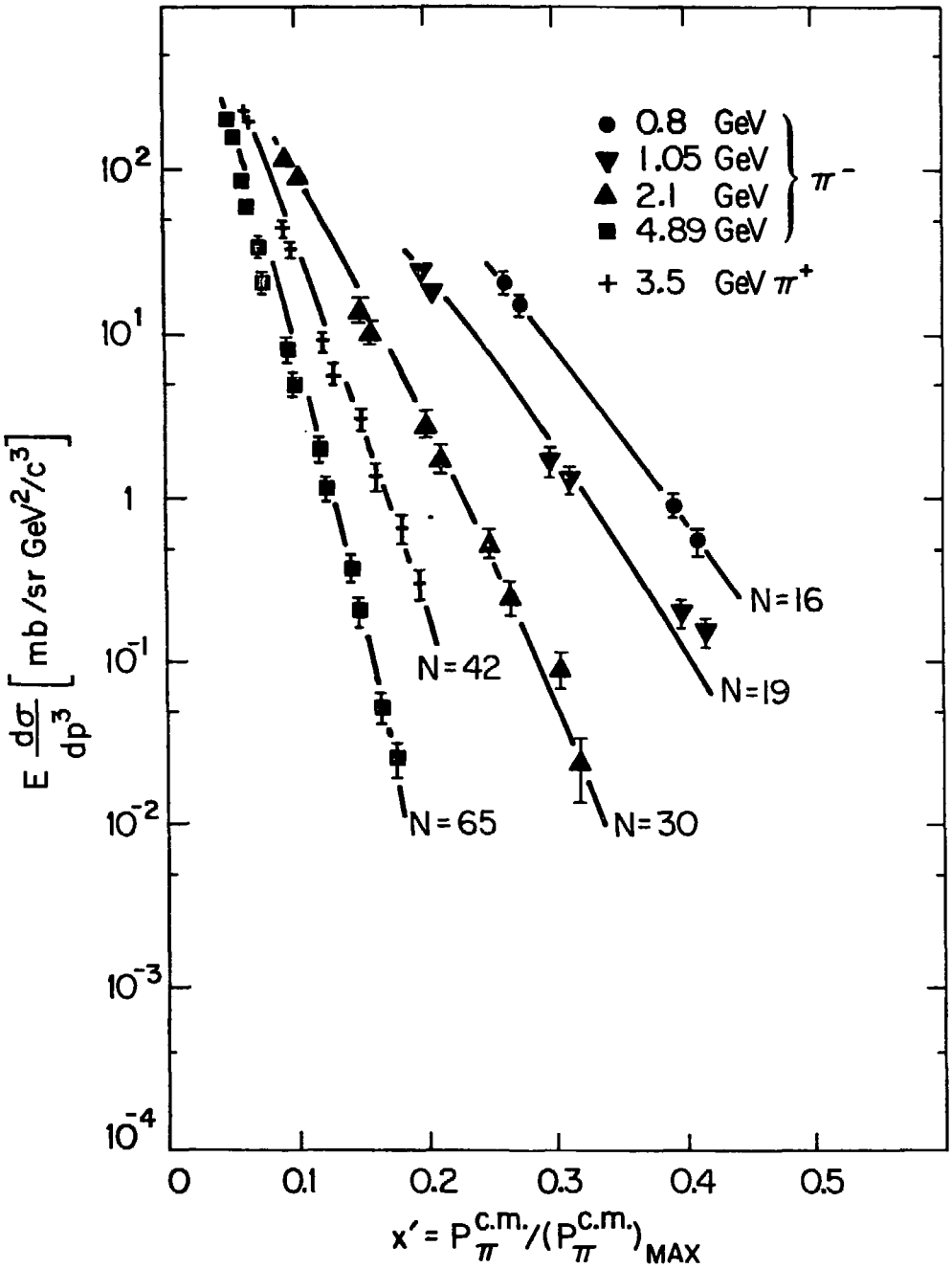

XBL 798 - 2505

Fig. 32

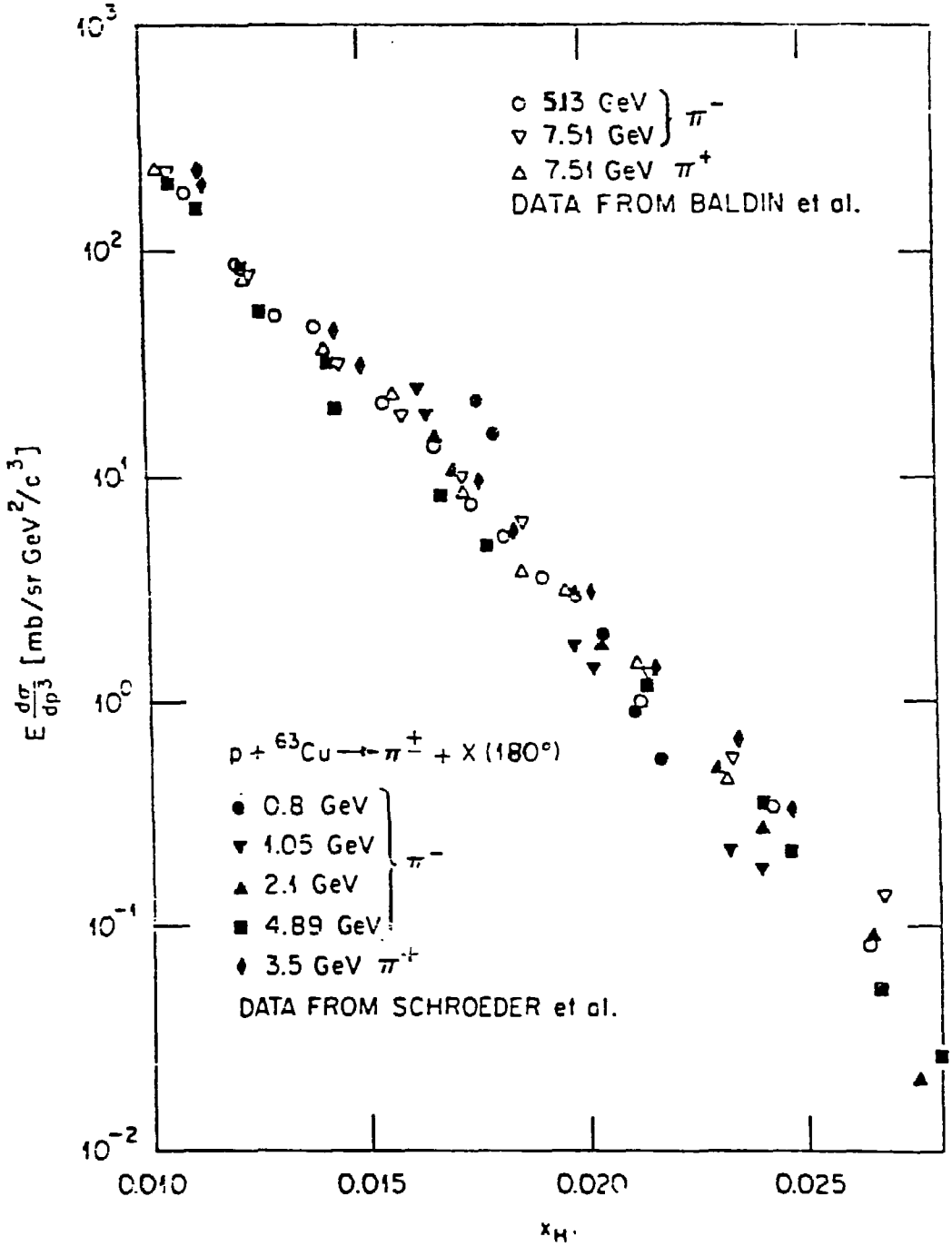
○ 5.13 GeV
▽ 7.51 GeV
π⁻
△ 7.51 GeV π⁺
DATA FROM BALDIN et al.
p + ⁶³Cu → π± + X (180°)
● 0.8 GeV
▼ 1.05 GeV
▲ 2.1 GeV
■ 4.89 GeV
π⁻
♦ 3.5 GeV π⁺
DATA FROM SCHROEDER et al.
E dσ/dp³ [mb/sr GeV²/c³]
x_H
10³
10²
10¹
10⁰
10⁻¹
10⁻²
0.010
0.015
0.020
0.025

Fig.33

ROLL 100
FRAME 6
B.T. 1
OP. NO.69
EXP. 61
EVT. 106
VIEW 1

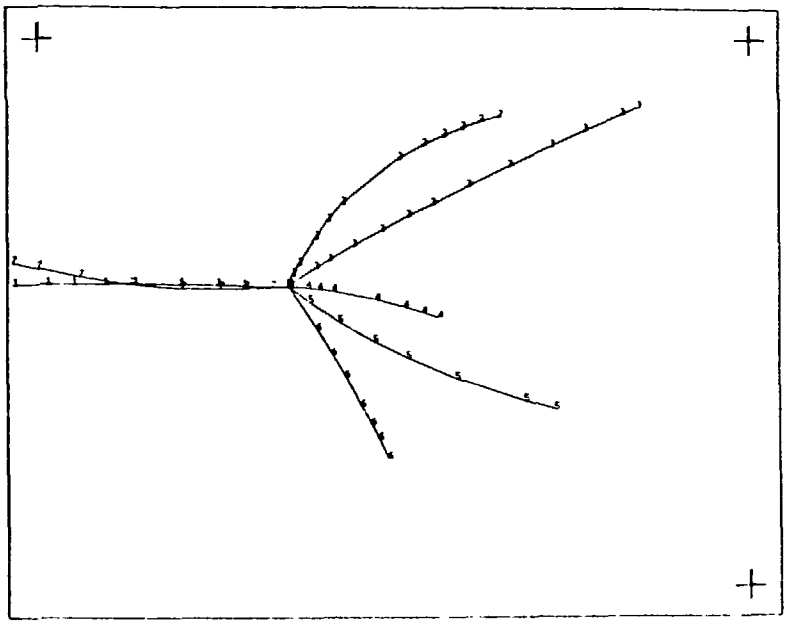

Fig. 34

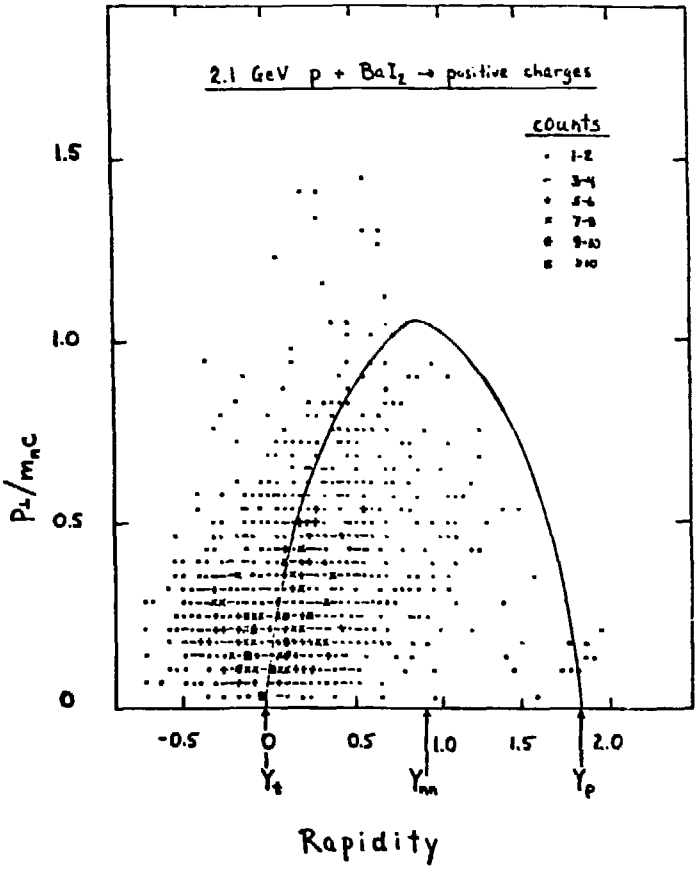
2.1 GeV p + BaI2 → positive charges
counts
1-2
3-4
5-6
7-8
9-10
>10
1.5
1.0
0.5
0
P⊥/mnc
-0.5
0
0.5
1.0
1.5
2.0
Yt
Ymn
Yp
Rapidity

Fig. 35

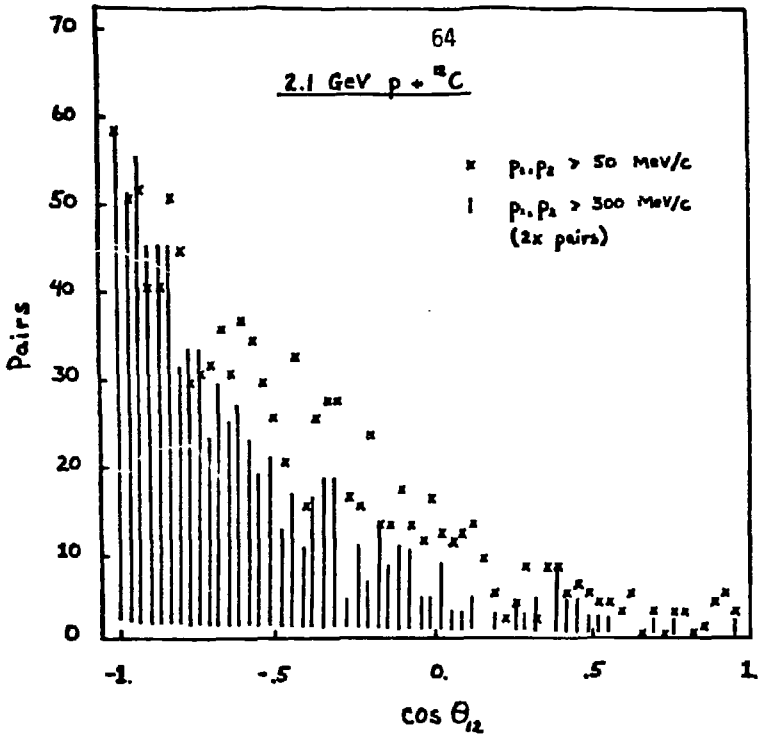
2.1 GeV p + 12C
x p1.p2 > 50 MeV/c
I p1.p2 > 300 MeV/c
(2x pairs)
Pairs
cos θ12
70
60
50
40
30
20
10
0
-1.
-.5
0.
.5
1.

Fig. 36

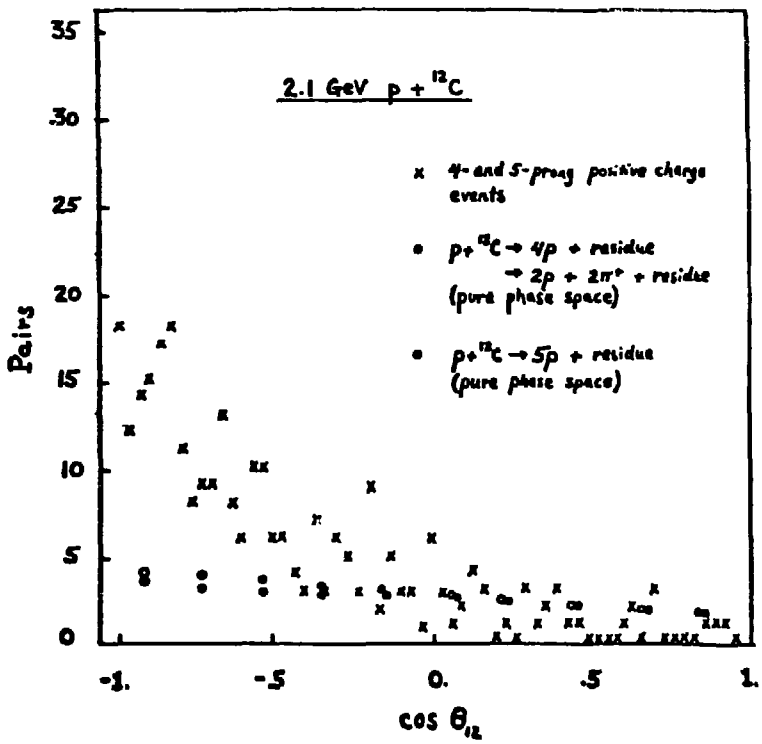
2.1 GeV p + 12C
x 4- and 5-prong positive charge events
• p+12C → 4p + residue
→ 2p + 2π+ + residue
(pure phase space)
• p+12C → 5p + residue
(pure phase space)
Pairs
cos θ12
35
30
25
20
15
10
5
0
-1.
-.5
0.
.5
1.

Fig. 37